Geochemistry Geophysics Geosystems G3
AN ELECTRONIC JOURNAL OF THE EARTH SCIENCES
Published by AGU and the Geochemical Society

Article
Volume 3, Number 11
16 November 2002
1065, doi:10.1029/2002GC000332
ISSN: 1525-2027

Origin of mafic magmas beneath northwestern Tibet: Constraints from ^{230}Th-^{238}U disequilibria

Kari M. Cooper
Department of Earth and Space Sciences, University of California-Los Angeles, 595 Charles Young Drive East, Los Angeles, California 90095-1567, USA

Now at Division of Geological and Planetary Sciences, California Institute of Technology, MC170-25, 1200 E. California Boulevard, Pasadena, California 91125, USA. (cooper@gps.caltech.edu)

Mary R. Reid
Department of Earth and Space Sciences, University of California-Los Angeles, 595 Charles Young Drive East, Los Angeles, California 90095-1567, USA

N. W. Dunbar and W. C. McIntosh
Earth and Environmental Science Department, New Mexico Bureau of Mines and Mineral Resources/New Mexico Tech, 801 Leroy Place, Socorro, New Mexico 87801-4796, USA

[1] ^{238}U-^{230}Th disequilibria and Sr, Nd, and Pb isotopic and chemical data for young (<120 ka) trachyandesites from the Ashikule Basin (AKB) in northwestern Tibet provide constraints on the origin of magmas produced within this region of continental collision. Compared to lavas from both continental and oceanic settings, the AKB samples show large excesses of ^{230}Th with respect to ^{238}U (up to $(^{230}\text{Th})/(^{238}\text{U}) = 1.36$). Partial melting of garnet-bearing lithologies (garnet peridotite, garnet pyroxenite, or eclogite) could be responsible for these ^{230}Th excesses and could plausibly occur either in the lithospheric mantle or in the lower crust. Small porosities (<0.4%) and slow melting rates ($<10^{-4}$ kg m^{-3} yr^{-1}) are required in the case of a garnet peridotite residue, although larger porosities (up to 18%) and melting rates ($>10^{-3}$ kg m^{-3} yr^{-1}) are permitted in the case of an eclogitic residue; hydrous metasomatic phases, if present, would lower these limits further. The source of the AKB magmas has probably been enriched in incompatible elements relative to bulk Earth since at least the middle Proterozoic (>1 Ga), likely via metasomatism by a relatively dry silicate melt, and, if the ultimate source of the lavas is mantle lithosphere, concentrations of incompatible trace elements in the source could be similar to those of xenoliths and massifs. The ^{230}Th-^{238}U disequilibria provide additional information to evaluate the methods previously proposed to explain melt generation beneath northern Tibet. The measured ^{230}Th enrichments are uncharacteristic of melts generated by subduction but could potentially be produced during shear heating of the uppermost lithospheric mantle, by convective removal of the lower lithosphere and heating of the remaining lithospheric mantle, or by decompression during extension across a releasing bend of a strike-slip fault. The diversity of mechanisms that could be responsible for these relatively small-degree melts suggests that the cause of melt production may have varied over time and/or over space in northwestern Tibet and therefore that timing of volcanism may not be directly related to any single tectonic event.

Components: 12,997 words, 5 figures, 2 tables.

Keywords: Tibetan plateau; continental magmatism; U-Th disequilibria; isotope geochemistry; melt generation; lithospheric mantle.

Index Terms: 3640 Mineralogy and Petrology: Igneous petrology; 1040 Geochemistry: Isotopic composition/chemistry; 8102 Tectonophysics: Continental contractional orogenic belts.

Received 15 February 2002; **Revised** 3 July 2002; **Accepted** 10 July 2002; **Published** 16 November 2002.

Cooper, K. M., M. R. Reid, N. W. Dunbar, and W. C. McIntosh, Origin of mafic magmas beneath northwestern Tibet: Constraints from ^{230}Th-^{238}U disequilibria, *Geochem. Geophys. Geosyst.*, *3*(11), 1065, doi:10.1029/2002GC000332, 2002.

1. Introduction

[2] Postcollisional volcanic activity on the Tibetan Plateau is volumetrically limited but geographically widespread [e.g., *Deng*, 1993; *Turner et al.*, 1996]. The Tibetan plateau is the site of ongoing continental collision, differing in that respect from the lithospheric thinning and asthenospheric upwelling that characterize many settings of continental volcanism. In north-central Tibet, the middle portion of the 55–60 km thick crust has been inferred to be partially molten based on an anomalously high Poisson's ratio [e.g., *Owens and Zandt*, 1997; *Kosarev et al.*, 1999]. Several mechanisms have been proposed to explain the enigmatic magmatism associated with the Tibetan plateau, including fluid-induced melting related to intracontinental subduction [*Arnaud et al.*, 1992; *Hacker et al.*, 2000; *Tapponnier et al.*, 2001], heating and melting of the lithospheric mantle as a result of catastrophic removal or thermal erosion of the lower lithosphere (i.e., the mechanical boundary layer) [*Arnaud et al.*, 1992; *Molnar et al.*, 1993; *Turner et al.*, 1993], and shear-induced heating leading to melting of the uppermost lithospheric mantle during deformation [*Kincaid and Silver*, 1996]. The chemical characteristics and timing of postcollisional volcanism on the Tibetan plateau have been used as evidence of the thermal and compositional structure of the lithosphere, and the timing and process of plateau growth [e.g., *Arnaud et al.*, 1992; *Turner et al.*, 1993, 1996; *Tapponnier et al.*, 2001]; thus, a better understanding of the process of melt generation is an important constraint for tectonic models.

[3] Trachyandesites from the Ashikule Basin (AKB) of northwestern Tibet are chemically and isotopically similar to other Tibetan lavas [cf. *Turner et al.*, 1996; *Miller et al.*, 1999], which are generally potassic, strongly enriched in incompatible elements, and have Nd and Pb isotope ratios suggesting that enrichment in incompatible elements is a characteristic of the source of the magmas [e.g., *Arnaud et al.*, 1992; *Deng*, 1993, 1998; *Turner et al.*, 1996]. In this paper, we present ^{238}U-^{230}Th disequilibrium and other isotopic analyses for these trachyandesites, virtually the only lavas on the Tibetan plateau known to be young enough (<~400 ka) to preserve U-Th disequilibria [*Deng*, 1998]. The magnitude of disequilibria in volcanic rocks between the activity (conventionally denoted by parentheses) of ^{238}U and its long-lived radioactive daughter ^{230}Th is controlled by, and thus may be used to extract information about, the processes of melt generation and transport. Therefore, melting constraints inferred from disequilibria in the AKB lavas may exemplify those responsible for melt generation in other areas of northern Tibet, and potentially other continental volcanic rocks in similar structural settings (e.g., potassic mafic to intermediate lavas along the North Anatolian Fault zone in Turkey) [*Adiyaman et al.*, 2001]. In addition, the common spatial association of Tibetan volcanic rocks and faults raises the possibility that melt generation is causally connected to fault motion and we assess the possibility that melting occurs as a result of extension across releasing bends in strike-slip faults.

2. Tectonic Setting

[4] The AKB is located within the western Kunlun Shan, an actively deforming mountain belt that forms the northwestern margin of the Tibetan Plateau (Figure 1). The basin contains several silicic domes (450–500 and 250–300 ka) and trachyandesitic flows (250–300 and 66–120 ka) [*Dunbar et al.*, 1996]. The trachyandesites have

extremely high abundances of incompatible elements (e.g., La concentrations are 164–196 ppm, ~450–600 times chondritic values; Table 2), and are chemically similar to other mafic volcanic rocks from northwestern Tibet [*Arnaud et al.*, 1992; *Turner et al.*, 1996], and elsewhere on the plateau [*Coulon et al.*, 1986; *Pearce and Mei*, 1988; *McKenna and Walker*, 1990; *Turner et al.*, 1996; *Miller et al.*, 1999].

[5] The structural history of the western Kunlun Shan is complex. The area roughly corresponds to the intersection of three major strike-slip systems: the Altyn Tagh, the Karakax, and the Ghoza-Longmu Co (Figure 1) and, in a broad sense, represents a boundary between the Tarim lithospheric block to the north and the terranes which make up the Tibetan plateau to the south. Collisions of lithospheric blocks in the area that is now the western Kunlun Shan occurred at approximately 450–380 and 180 Ma [*Matte et al.*, 1996; *Mattern et al.*, 1996; *Yin and Nie*, 1996; *Yin and Harrison*, 2000; *Cowgill*, 2001]. Furthermore, the Tarim lithosphere may currently be subducting southward beneath the Tibetan plateau [*Lyon-Caen and Molnar*, 1984], in which case the AKB may be underlain at depth by Tarim lithosphere. Whatever its affinity, the lithosphere underlying the AKB is likely Precambrian in age [*Sengor*, 1985; *Dewey et al.*, 1988; *Yin and Nie*, 1996].

3. Results

[6] We measured Th, Pb, Nd, and Sr isotopic ratios and Th and U concentrations in samples from the younger episode of mafic volcanism in the AKB. Analyses were performed by TIMS at UCLA; analytical methods, including typical blanks (negligible considering the sample size and high abundance of trace elements in AKB samples), are described in de-tail elsewhere [*Reid*, 1995; *Reid and Ramos*, 1996]. Values for the standards are reported in Table 1. External reproducibility of Th isotope analyses for these samples can be assessed by duplicate analyses in Table 1 and was better than 2% (2σ); reproducibility of U/Th ratios is estimated to be better than 2% [*Reid and Ramos*, 1996]. Major and trace element analyses of the same powders were performed at the New Mexico Institute of Mining and Technology (Table 2).

[7] The rocks are potassic (K_2O = 4.0–4.4 wt.%) trachyandesites and basaltic trachyandesites. Age-corrected (^{230}Th)/(^{232}Th) ratios are near the lower limit of those observed globally, and fall within the range of values for continental basalts that elsewhere have been attributed to derivation from lithospheric mantle sources [*Williams et al.*, 1992; *Reid and Ramos*, 1996; *Asmerom*, 1999]. Notably, the ratios do not overlap the fields for midocean ridge basalts (MORB), ocean island basalts (OIB), or subduction-related volcanic rocks (Figure 2). Age-corrected (^{230}Th)/(^{238}U) values for AKB lavas are relatively high (1.07–1.36) compared to lavas from both continental and oceanic settings, implying significant fractionation of Th from U during magma genesis. In general, age-corrected (^{230}Th)/(^{232}Th) and (^{230}Th)/(^{238}U) in the Ashikule samples decrease with increasing eruption age (Tables 1 and 2). Pb, Nd and Sr isotope data for the AKB mafic lavas (Table 1) are similar to values reported for other Tibetan lavas [cf. *Arnaud et al.*, 1992; *Deng*, 1993; 1998; *Turner et al.*, 1996]. High $^{207}Pb/^{204}Pb$ values with respect to $^{206}Pb/^{204}Pb$ suggest enrichment of the Ashikule source during the Archean [cf. *Turner et al.*, 1996]. Time-integrated $^{232}Th/^{238}U$ in the source calculated for >3 Ga of ingrowth of the Pb isotope characteristics (κ(Pb)), is ~4.1, somewhat lower than $^{232}Th/^{238}U$ in equilibrium with initial (^{230}Th)/(^{232}Th) (κ(Th) = 4.6–5.7; Table 1). The Ashikule lavas have lower $^{143}Nd/^{144}Nd$ and higher $^{87}Sr/^{86}Sr$ than oceanic island basalts (Table 1), characteristics generally similar to the EMII end-member of *Zindler and Hart* [1986] and consistent with derivation from an ancient, large ion lithophile-enriched source.

4. Discussion

4.1. Melting Parameters for AKB Lavas

[8] Any source of magmas that has remained closed to Th and U for more than ~400 kyears will be analytically indistinguishable from secular equilibrium, where the activity ratio (^{230}Th)/(^{238}U) = 1. The strong Th enrichment of the AKB lavas reflects fractionation of U from Th and could have been produced during partial melt-

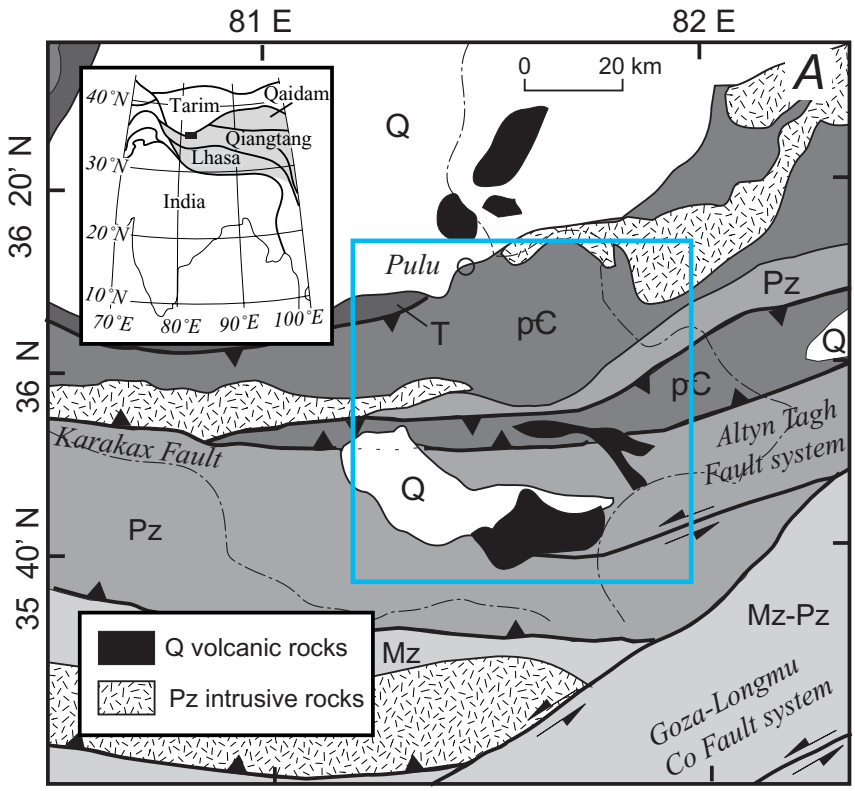
81 E
82 E
36 20' N
36 N
35 40' N
0 20 km
A
Q
Pulu
T
pC
Pz
Q
pC
Altyn Tagh Fault system
Karakax Fault
Q
Pz
Mz-Pz
Mz
Goza-Longmu Co Fault system
Q volcanic rocks
Pz intrusive rocks
40°N
30°N
20°N
10°N
70°E
80°E
90°E
100°E
Tarim
Qaidam
Qiangtang
Lhasa
India

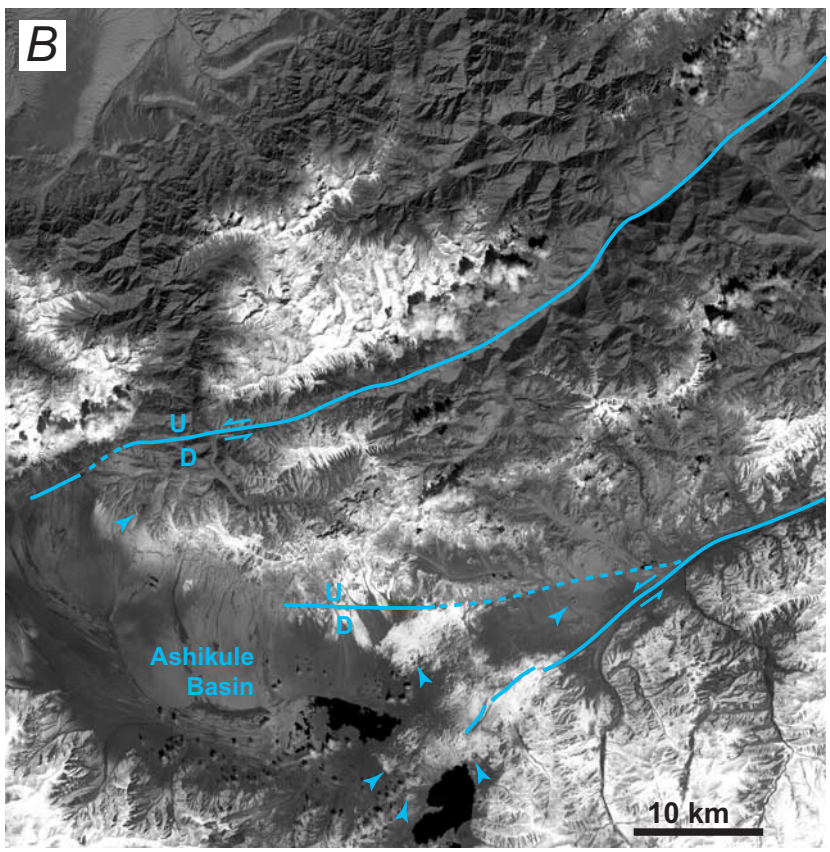
B
U
D
U
D
Ashikule Basin
10 km

ing or potentially during differentiation of the lavas. Wholesale assimilation of crustal material [cf. *Reid*, 1995] is unlikely to have increased (^{230}Th)/(^{238}U) in the AKB lavas because basement rocks, including plutons as young as ~250 ka, will be in or nearly in secular equilibrium. For the high (^{230}Th)/(^{238}U) in the liquid to be the product of differentiation would require a fractionating phase assemblage that preferentially sequesters U compared to Th, which could be the case if a significant proportion of zircon or apatite fractionated. However, zircon saturation temperatures calculated for the AKB lavas (using the method of *Watson and Harrison* [1983]) range from 785°C to 825°C, well below apatite saturation temperatures of ~1050°C which are more like expected eruption temperatures for these compositions. In addition, Zr increases with decreasing MgO in the sample suite (Table 2) (N. Dunbar, unpublished data), the opposite of what would be expected for significant zircon fractionation. A large mass fraction of apatite would have to be fractionated in order to greatly change (^{230}Th)/(^{238}U) in the residual liquid (e.g., 5–10% fractional crystallization of apatite would increase (^{230}Th)/(^{238}U) in the residual liquid from 1.2 to 1.3), which would require an additional 2–4 wt.% P_2O_5 in the parental liquid. Thus, we attribute the high (^{230}Th)/(^{238}U) of the AKB lavas to partial melting, either that in the source of the magmas or related to crustal assimilation.

[9] The degree of disequilibrium generated during melting is a function of the mineralogy of the source and the process of melt generation and thus, unless greatly modified during transport, disequilibria in erupted lavas contain important information about melt genesis. Compared to other continental basalts, the magnitude of Th enrichment in the AKB lavas is quite variable. Sr, Nd, and Pb isotopic compositions and incompatible element abundances between all Ashikule trachyandesites are, however, quite similar, which suggests the range of ^{230}Th excesses is not the result of variable contributions from isotopically distinct sources (e.g., mantle versus crust). Time spent in a crustal reservoir would decrease the disequilibria in the magmas through decay of ^{230}Th and may ultimately be responsible for the lower (^{230}Th)/(^{238}U) measured in some of the trachyandesites. For this reason, in this section we explore the conditions necessary to produce the more extreme disequilibria measured in AKB lavas.

4.1.1. Melting Models

[10] A signature feature of the AKB trachyandesites is the extreme magnitude of Th enrichment (Figure 2). In general, greater (^{230}Th)/(^{238}U) can be achieved by syn-melting ^{230}Th ingrowth than by fractionation during batch melting because decay of ^{238}U, preferentially retained in the solid residue, can continue to increase ^{230}Th/^{238}U in the melt during the period of time where the melt is in equilibrium with the residue [e.g., *Elliott*, 1997]. Dynamic melting models assume that melting occurs due to adiabatic decompression, that some critical melt fraction must be achieved before melt segregation can occur, and that any additional melt produced beyond the critical melt fraction is immediately extracted from the source and pooled elsewhere prior to eruption [*McKenzie*, 1985; *Williams and Gill*, 1989; *Zou and Zindler*, 2000]. "Continuous melting" [*McKenzie*, 1985; *Williams and Gill*, 1989] is similar to dynamic melting in that the source maintains a finite residual porosity, but differs in that the source is not upwelling. The magnitude of ^{230}Th-^{238}U disequilibria produced in these melting models is a function of the melting rate and the critical melt fraction in the melting region, as well as the bulk partition coefficients (D's) of U and Th in the source. Disequilibria

Figure 1. (opposite) (A) Simplified geologic map of the area surrounding the AKB, modified from the work of *Cowgill et al.* [2001, in preparation]; shaded areas indicate gneisses, metamorphosed sedimentary rocks, and sedimentary rocks grouped by age. Heavy lines denote faults and dot-dash lines represent rivers. Blue box indicates location of (B). The inset shows the major lithospheric blocks that make up the Tibetan plateau [*Yin and Nie*, 1996], with the shaded area indicating the geographic boundaries of the Tibetan plateau and the box indicating the location of (A). (B) ASTER satellite image of the AKB and surrounding areas showing location of Quaternary faults (heavy blue lines; dashed where approximately located) and volcanic vents (arrows). Vents may be seen more clearly by zooming in on the figure in the electronic version.

Table 1. Isotopic and Trace Element Data for AKB Samples

Sample[a]	$^{206}Pb/^{204}Pb$	$^{207}Pb/^{204}Pb$	$^{208}Pb/^{204}Pb$	Sm (ppm)	Nd (ppm)	$^{143}Nd/^{144}Nd$[b]	ε_{Nd}	$^{87}Sr/^{86}Sr$[b]	Th (ppm)	U (ppm)	$(^{230}Th)/(^{232}Th)$	$(^{230}Th)_0/(^{232}Th)$[c]	$(^{230}Th)_0/(^{232}Th)$ +/−[d]	$(^{230}Th)_0/(^{238}U)$[c]	$(^{230}Th)_0/(^{238}U)$ +/−[d]	$\kappa(Th)_0$[e]
AKB-1	18.789	15.681	39.102	19.864	142.64	0.512296	−6.66	0.710309	25.99	4.72	0.581	0.625	+0.011/−0.010	1.135	+0.019/−0.018	5.0
AKB-1A											0.583	0.631	+0.007/−0.007	1.145	+0.014/−0.013	5.0
AKB-2	18.738	15.654	38.962	18.143	129.34	0.512264	−7.30	0.710250	30.99	5.65	0.593	0.638	+0.009/−0.008	1.152	+0.016/−0.015	4.9
AKB-4	18.785	15.658	39.069	19.863	137.22	0.512273	−7.13	0.710360	34.72	5.80	0.588	0.669	+0.010/−0.010	1.354	+0.020/−0.019	4.7
AKB-4A											0.583	0.660	+0.012/−0.012	1.302	+0.024/−0.023	4.7
AKB-5	18.799	15.682	39.116	18.153	126.4	0.512235	−7.87	0.710351	30.29	5.18	0.583	0.636	+0.012/−0.012	1.226	+0.024/−0.023	4.9
AKB-6	18.758	15.659	39.014	19.927	139.12	0.512265	−7.28	0.710271	30.55	5.00	0.589	0.677	+0.007/−0.007	1.364	+0.015/−0.015	4.6
AKB-6A											0.588	0.674	+0.008/−0.008	1.358	+0.017/−0.016	4.7
AKB-10	18.747	15.693	39.001	22.222	155.52	0.512263	−7.32	0.710440	29.39	5.01	0.588	0.552	+0.012/−0.010	1.068	+0.024/−0.020	5.7

$^{230}Th/^{232}Th$ (±2σ) measured on a standard solution and on international reference samples using the same analytical procedure are UC Santa Cruz Th standard, 170587 (0.26%), n = 35; AGV1, 199040 (0.20%), n = 5; and JB1, 332302 (0.96%), n = 5.

[a] Sample names followed by "A" indicate powder replicates of Th isotopic analyses.

[b] Normalization constants are $^{86}Sr/^{84}Sr = 0.1194$ and $^{146}Nd/^{144}Nd = 0.7219$.

[c] Activities of ^{230}Th corrected for posteruptive decay. Activities calculated using the following decay constants (all per year): $\lambda_{230} = 9.1952 \times 10^{-6}$, $\lambda_{232} = 4.9475 \times 10^{-11}$, and $\lambda_{238} = 1.5513 \times 10^{-10}$.

[d] Propagated uncertainties in initial $(^{230}Th)/(^{232}Th)$ and $(^{230}Th)/(^{238}U)$ ratios including analytical errors (2σ) in $^{230}Th/^{232}Th$ and 1σ errors in eruption ages.

[e] $\kappa(Th) = {}^{232}Th/^{238}U$ (atom ratio) calculated from measured $^{230}Th/^{232}Th$ (corrected for posteruptive decay) by assuming that activities of ^{230}Th and ^{238}U are equal.

Table 2. Major and Trace Element Data for AKB Samples

Sample	AKB-1	AKB-2	AKB-4	AKB-5	AKB-6	AKB-10
Eruption Age (ka)[a]	100 ± 3	83 ± 2	76 ± 3	66 ± 1	72 ± 1	122 ± 8
SiO_2	54.7	57.2	57.3	52.3	56.8	55.5
TiO_2	1.91	1.81	1.89	1.72	1.95	2.19
Al_2O_3	14.1	14.5	14.3	13.3	14.7	14.5
Fe_2O_3	7.58	7.07	7.15	6.65	7.58	7.71
MnO	0.12	0.11	0.10	0.10	0.11	0.12
MgO	3.75	2.89	3.32	3.06	3.44	2.77
CaO	6.79	5.87	5.95	8.11	5.85	5.95
Na_2O	2.41	2.32	2.88	2.77	3.02	3.13
K_2O	4.02	4.29	4.37	4.01	4.31	4.01
P_2O_5	1.11	0.95	1.00	0.93	1.05	1.19
LOI	2.41	1.89	1.64	4.86	0.70	1.72
Total	99.89	98.86	99.93	97.84	99.47	98.76
Sc	11.08	9.62	–	–	–	9.4
Cr	64.7	32.3	–	–	–	19
Co	34.5	30.1	–	–	–	26.01
Zn	118	128.5	–	–	–	139
As	3	3.5	–	–	–	2.2
Br	2.7	1.42	–	–	–	1.3
Rb	130	150	–	–	–	147
Sr	1196	1201	–	–	–	1274
Zr	485	557	–	–	–	647
Sb	0.074	0.059	–	–	–	0.033
Cs	3.14	5.32	–	–	–	2.62
Ba	2164	2052	–	–	–	2032
La	168.8	164.8	–	–	–	196.7
Ce	330	328	–	–	–	384
Nd	127	136	–	–	–	146
Sm	20.04	19.42	–	–	–	22.03
Eu	4.13	3.87	–	–	–	4.28
Tb	1.409	1.414	–	–	–	1.536
Yb	2.02	2.06	–	–	–	2
Lu	0.23	0.233	–	–	–	0.256
Hf	12.18	13.78	–	–	–	15.12
Ta	2.46	2.6	–	–	–	2.83
W	82	63	–	–	–	48.3
Th	28.58	30.5	–	–	–	29.08
U	4.5	5.81	–	–	–	5.6

Major-element analyses (wt.%) were made with a Rigaku 3062 XRF instrument at New Mexico Institute of Mining and Technology. Errors, in weight percent, based on replicate analyses of internal standard reference material are SiO_2 ±0.16, TiO_2 ±0.01, Al_2O_3 ±0.03, Fe_2O_3 ±0.01, MnO ±0.04, MgO ±0.04, CaO ±0.11, Na_2O ±0.04, K_2O ±0.03, and P_2O_5 ±0.01.

Trace element analyses were made by neutron activation analysis at New Mexico Institute of Mining and Technology. Analytical errors, in ppm, based on replicate analyses of internal reference material are Ba ±10, La ±1.8, Ce ±1.4, Nd ±0.7, Sm ±0.07, Eu ±0.14, Tb ±0.02, Yb ±0.07, Lu ±0.01, Hf ±0.12, Ta ±0.04, W ±0.05, Th ±1, and U ±0.5.

[a] Eruption ages (±1σ) uncertainties ($^{40}Ar/^{39}Ar$ analyses of sanidine crystals) from W. C. McIntosh and N. Dunbar (unpublished data).

produced by dynamic and continuous melting models are similar at fast melting rates and/or small total melt fractions, whereas at slower melting rates or larger melt fractions a continuous melt will have lower (^{230}Th)/(^{238}U) than a dynamic melt under the same conditions [*Williams and Gill*, 1989]. Because it defines the most generous (i.e., maximum porosity, minimum melting rate) conditions necessary to produce the ^{230}Th excesses measured in AKB samples, we model dynamic melting explicitly here [*Zou and Zindler*, 2000] even though not all conceptual models of melt production beneath Tibet require melting via adiabatic decompression (see section 5.2).

4.1.2. Melting of Anhydrous Lithosphere

[11] Enrichment of ^{230}Th relative to ^{238}U requires melting in the presence of a residual phase that

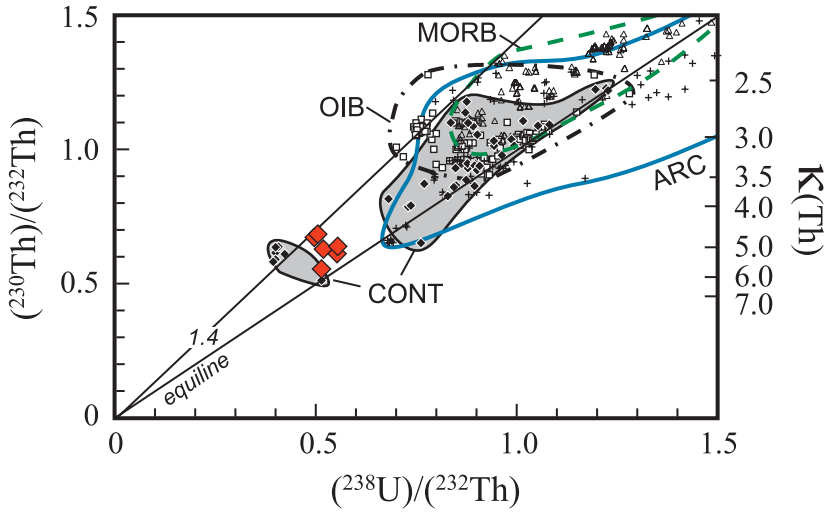

Figure 2. ^{230}Th-^{238}U isochron diagram showing the data for AKB samples (large red diamonds); measurement uncertainty is smaller than the size of the symbols and data are shown corrected for posteruptive decay of ^{230}Th. Also shown are fields for MORBs (open triangles), OIBs (open squares), subduction-related lavas (ARC; crosses), and other continental intraplate lavas (CONT; small black diamonds). The small group closer to the origin represents the Gaussberg lamproites analyzed by *Williams et al.* [1992]; these are plotted separately because they are significantly different both in bulk composition and in Th-isotope composition from the other continental lavas. Fine black lines indicate (^{230}Th)/(^{238}U) = 1 (the equiline) and (^{230}Th)/(^{238}U) = 1.4 (labeled). Also shown along right-hand axis are values for ^{232}Th/^{238}U in equilibrium with (^{230}Th)/(^{232}Th) (κ(Th)). Ingrowth of ^{230}Th during melting will lead to elevated (^{230}Th)/(^{232}Th) compared to that in equilibrium with ^{238}U/^{232}Th in the source, implying that if ingrowth has occurred κ(Th) will underestimate Th/U in the source. MORB data were compiled partly by using the PetDB database (28 August 2001, http://petdb.ldeo.columbia.edu/petdb/query.asp) [*Goldstein et al.*, 1989, 1991; *Bourdon et al.*, 1996a, 2000; *Lundstrom et al.*, 1999; *Sturm et al.*, 2000]. Other data from the following sources: *Williams and Gill* [1992], *Condomines and Sigmarsson* [1993], *Gill et al.* [1993], *Goldstein et al.* [1993], *Volpe and Goldstein* [1993], *Chabaux and Allegre* [1994], *Asmerom and Edwards* [1995], *Condomines et al.* [1995], *Reid* [1995], *Sims et al.* [1995, 1999], *Cohen et al.* [1996], *Reid and Ramos* [1996], *Huang et al.* [1997], *Pickett and Murrell* [1997], *Clark et al.* [1998], *Claude-Ivanaj et al.* [1998], *Chabaux et al.* [1999], *Gauthier and Condomines* [1999], *Thomas et al.* [1999], *Turner et al.* [2000b], *Zellmer et al.* [2000], *Cooper et al.* [2001], and *Pietruszka et al.* [2001].

preferentially retains U compared to Th (i.e., $D_U > D_{Th}$); the most likely candidate for this, considering the large ^{230}Th enrichments in the AKB lavas, is garnet [*Beattie*, 1993; *LaTourrette et al.*, 1993; *Salters and Longhi*, 1999]. Garnet might be present in both primary (i.e., peridotite) and secondary (e.g., pyroxenite and eclogite) mantle assemblages as well as in the lower crust. The results of dynamic melting calculations for garnet-bearing mafic and ultramafic lithologies are shown in Figure 3; the curves in Figure 3A illustrate combinations of maximum porosity and melting rate that will produce a given (^{230}Th)/(^{238}U) ratio which, for the AKB lavas, is 1.36, the maximum disequilibria measured. Use of an equilibrium porous flow model [*Spiegelman and Elliott*, 1993; *Lundstrom et al.*, 1995] will result in somewhat higher maximum porosities and/or melting rates than these [e.g., *Sims et al.*, 1999; *Pietruszka et al.*, 2001]. Because radioactive decay during transport would reduce (^{230}Th)/(^{238}U), lower porosity and/or slower melting could also be responsible for the lavas. For a given source mineralogy there is a tradeoff between the maximum critical volume porosity and the maximum melting rate that will produce a given (^{230}Th)/(^{238}U) ratio. For example, melting of a garnet peridotite source at rates of $>10^{-6}$ kg m^{-3} yr^{-1} requires porosities of <0.4% to produce (^{230}Th)/(^{238}U) $\geq$1.36 in the melt. Because of their higher modal percentage of garnet, pyroxenitic and eclogitic sources are permissive of larger porosities (e.g., 2%) and/or faster melting than a peridotite source for a given set of partition coefficients [i.e., *Salters and Longhi*, 1999] (Figure 3). Use of

different partition coefficients for clinopyroxene [*Lundstrom et al.*, 1994] and garnet [*van Westrenen et al.*, 1999], which may be more representative of eclogitic bulk compositions [e.g., *Stracke et al.*, 1999; *van Westrenen et al.*, 2001], permits even larger porosities (up to 18%) and faster melting rates. Thus, partial melting of either mantle or mafic crustal assemblages could be responsible for Th enrichments in the AKB lavas.

[12] Recent work has shown that residual clinopyroxene in the absence of garnet at pressures >1.5 GPa (e.g., partial melting of spinel peridotite) can also produce melts with $(^{230}Th)/(^{238}U) > 1$ [*Wood et al.*, 1999; *Turner et al.*, 2000a; *Landwehr et al.*, 2001]. However, generating Th excesses comparable to those measured in the AKB in melts of a spinel peridotite source would require extremely small residual porosities (0.001%) at slow melting rates (10^{-5} kg m^{-3} yr^{-1}), even when the more generous case of equilibrium porous flow is assumed [*Landwehr et al.*, 2001]. Therefore, we consider garnet-bearing lithologies to be more likely sources for the AKB magmas.

[13] Partial melts of intermediate to silicic lower crustal assemblages are not included in Figure 3 because they are likely to be more evolved in composition than the trachyandesites [e.g., *Patiño Douce and Beard*, 1995; *Patiño Douce and McCarthy*, 1998]. However, partial melts of such lithologies could have contributed to the AKB magmas, either in the melting region or by interaction of more mafic parental magmas with crust during transport to the surface. Attributing the high $(^{230}Th)/(^{238}U)$ ratios in AKB lavas to such interactions while maintaining their relatively mafic bulk compositions would require an assimilant with both higher concentrations of Th and U and significantly higher $(^{230}Th)/(^{238}U)$ than the AKB lavas. Although residual garnet or zircon could potentially produce silicic melts with $(^{230}Th)/(^{238}U) > 1$, no data have been reported to date for rhyolites with $(^{230}Th)/(^{238}U) > 1.36$. Attributing the high $(^{230}Th)/(^{238}U)$ in the AKB magmas instead to assimilation of partial melts of mafic crustal lithologies would require even more extreme limitations on conditions of melting than discussed above (Figure 3).

[14] The melting rate/porosity combinations shown in Figure 3 are conservative maxima for dynamic partial melting because (1) use of other D's [e.g., *LaTourrette and Burnett*, 1992; *Hauri et al.*, 1994; *Lundstrom et al.*, 1994; *Wood et al.*, 1999; *Landwehr et al.*, 2001], mixing with spinel-peridotite melts, and decay of ^{230}Th during melt transport and storage will all decrease $(^{230}Th)/(^{238}U)$ measured in the volcanic rocks compared to our model parameters; (2) chemical exchange of melts produced by dy-namic melting with the mantle or crust during magmatic ascent [e.g., *Spiegelman and Elliott*, 1993] would likely reduce the disequilibrium because the majority of the crust and mantle traversed would not contain garnet [e.g., *Lundstrom et al.*, 1995; *Bourdon et al.*, 1996b]; and (3) disequilibrium melting would also likely decrease $(^{230}Th)/(^{238}U)$ over that produced by equilibrium melting unless Th diffusion in mantle phases is significantly faster than diffusion of U [*Qin*, 1992]. Th and U diffusivities in diopside appear to be similar and quite slow [*Van Orman et al.*, 1998] and, assuming that this relationship holds for garnet as well, it is likely that chemical equilibrium will be attained only in cases of very slow melting. Therefore, within the context of the dynamic melting model, the only conditions under which larger porosities and/or faster melting rates would be allowed would be at total melt fractions less than the values at which quasi steady state is reached (~1–2%; see Figure 3). In any case, the curves shown in Figure 3 are probably representative of relative differences in melting rate and porosity between different source mineralogies for a given $(^{230}Th)/(^{238}U)$ ratio.

[15] Also plotted in Figure 3 are curves representing the conditions that would be required to produce the magnitude of U-Th disequilibria measured in MORB and Hawaiian basalts by melting of garnet peridotite. The ranges of $(^{230}Th)/(^{238}U)$ measured in both MORB and OIBs are very large and overlap significantly (see Figure 2) but most MORB samples measured have relatively low $(^{230}Th)/(^{238}U)$ ratios (mean 1.09, 80% of analyses <1.25 in the compilation used here; see Figure 2 for references) whereas alkaline OIB in general have higher $(^{230}Th)/(^{238}U)$ ratios (mean value of 1.17 and 80% of analyses <1.35). Reference to Figure 3 shows that the AKB

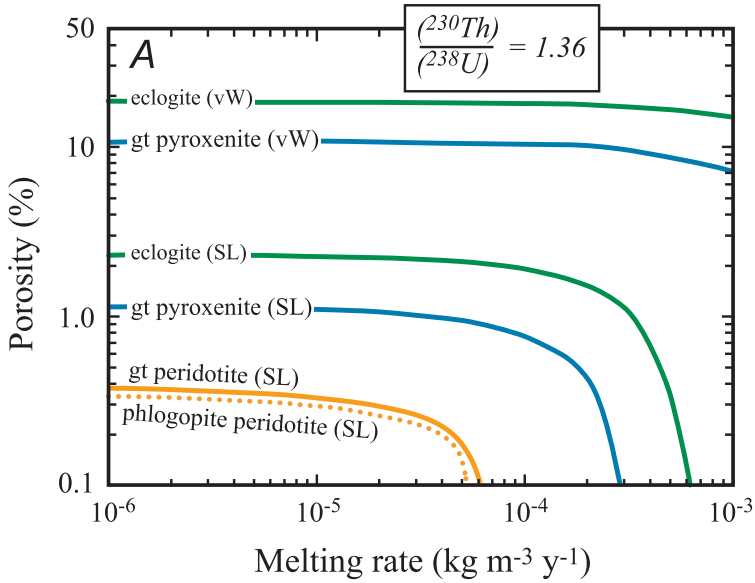
A
(230Th)/(238U) = 1.36
eclogite (vW)
gt pyroxenite (vW)
eclogite (SL)
gt pyroxenite (SL)
gt peridotite (SL)
phlogopite peridotite (SL)
Porosity (%)
50
10
1.0
0.1
10-6
10-5
10-4
10-3
Melting rate (kg m-3 y-1)

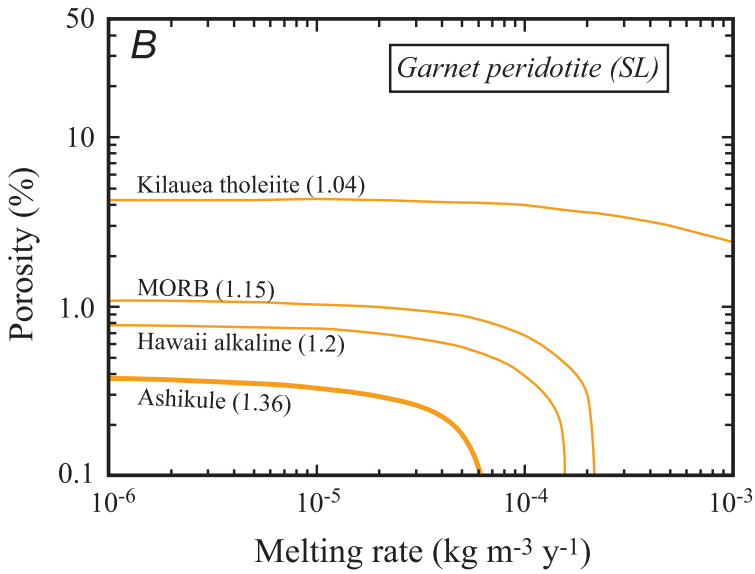
B
Garnet peridotite (SL)
Kilauea tholeiite (1.04)
MORB (1.15)
Hawaii alkaline (1.2)
Ashikule (1.36)
Porosity (%)
50
10
1.0
0.1
10-6
10-5
10-4
10-3
Melting rate (kg m-3 y-1)

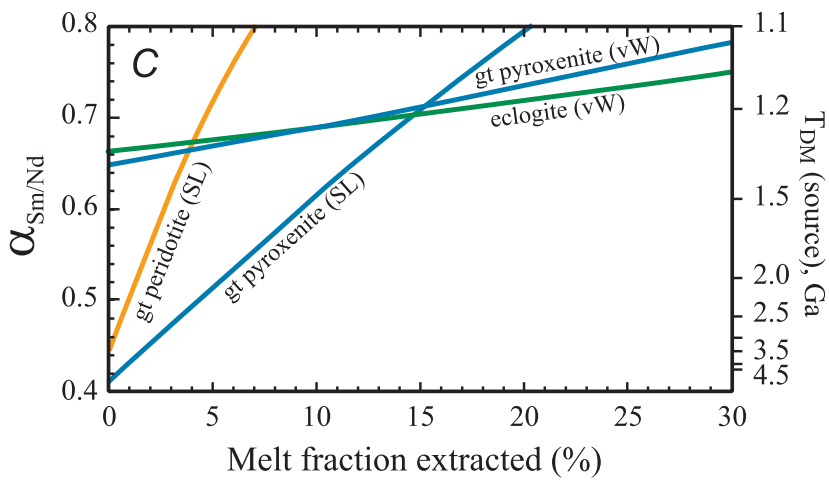
C
gt pyroxenite (vW)
eclogite (vW)
gt peridotite (SL)
gt pyroxenite (SL)
αSm/Nd
0.8
0.7
0.6
0.5
0.4
TDM (source), Ga
1.1
1.2
1.5
2.0
2.5
3.5
4.5
0
5
10
15
20
25
30
Melt fraction extracted (%)

lavas must represent some combination of lower residual porosity, lower melting rates, and/or greater influence of melts produced in the presence of garnet in their source region relative to the conditions and sources of melting beneath Hawaii or midocean ridges, although conditions of melting beneath other ocean islands (notably Grand Comore [*Claude-Ivanaj et al.*, 1998]) could be similar.

4.1.3. Effects of Hydrous Phases

[16] Judging by the variety of subduction-related events that could have affected them, the mantle lithosphere and lower crust of northwestern Tibet may have been metasomatized by hydrous or carbonic fluids or by silicate melts and previous work [*Turner et al.*, 1996; *Miller et al.*, 1999] has attributed origin of the Tibetan lavas to melting of a phlogopite-bearing source. Mineral/melt partition coefficients of U and Th in phlogopite and amphibole are very similar [*LaTourrette et al.*, 1995], such that equilibrium melting in the presence of refractory phlogopite or amphibole would require extraction of partial melts formed at even lower melting rates and/or porosities than those inferred for melting of an anhydrous assemblage. For comparison, a curve for modal melting of peridotite with 6% phlogopite [cf. *Turner et al.*, 1996] is also plotted in Figure 3A. A higher modal percentage of phlogopite in the assemblage and/or nonmodal melting where mica is preferentially melted would require

Figure 3. (opposite) (A) Results of forward modeling of ^{230}Th-^{238}U disequilibria produced during dynamic melting. Curves shown indicate combinations of maximum porosity and melting rate that will produce (^{230}Th)/(^{238}U) = 1.36, the maximum disequilibria measured in the AKB lavas, by partial melting of a specific lithology; lower porosity and/or slower melting result in higher ^{230}Th excesses. Curves were calculated using the equations of *Zou and Zindler* [2000]. The general behavior of the model is that the highest disequilibria are generated at very low melt fractions (<1%); as melting proceeds, the disequilibrium in the melt will decrease until a quasi steady state is achieved (at ~2% total melt extracted). After this point, (^{230}Th)/(^{238}U) in the melt will remain constant until either Th or U is entirely extracted from the melt. However, the absolute concentrations of Th and U in the melt will decrease by dilution as the fraction of melt extracted increases [cf. *Zou and Zindler*, 2000]. Curves shown are for extracted melt fractions of 3% (garnet and phlogopite peridotite and pyroxenite) or 25% (eclogite), broadly consistent with the melt fractions expected to produce basaltic to andesitic bulk compositions. As expected for steady state, curves for 5% or 10% melt extracted are virtually identical to those shown, differing only slightly at low porosities/high melting rates. Source lithologies have the following modal percentages (garnet/cpx/opx/olivine): garnet peridotite (solid orange line; 8:8:30:54), garnet pyroxenite (solid blue line; 30:70:0:0), eclogite (solid green line; 50:50:0:0), and phlogopite peridotite (dotted line; 7.5:7.5:28:51, the same relative proportions as in the anhydrous peridotite plus 6% phlogopite). Curves labeled "SL" are based on partition coefficients for clinopyroxene and garnet from high-pressure experiments of *Salters and Longhi* [1999] and phlogopite from experiments of *LaTourrette et al.* [1995]; partition coefficients for olivine and orthopyroxene were assumed to be zero. Curves for eclogite and pyroxenite labeled "vW" were calculated using partition coefficients of *van Westrenen et al.* [1999] for garnet and of *Lundstrom et al.* [1994] for clinopyroxene, which are likely more representative of the composition of these phases in pyroxenitic or eclogitic bulk compositions [e.g., *Stracke et al.*, 1999; *van Westrenen et al.*, 2001]. (B) Comparison between the maximum melting rate/porosity combinations necessary to produce disequilibria measured in AKB samples, Hawaiian tholeiite, and alkalai basalt (dashed lines) [*Sims et al.*, 1999; *Pietruszka et al.*, 2001] and in average of MORB data (dot-dash line) (see references in Figure 2). Mineralogy is assumed to be garnet peridotite using modal mineralogy and partition coefficients as described for (A). (C) Fractionation of Sm and Nd ($\alpha_{Sm/Nd}$, defined as $(Sm/Nd)_{melt}/(Sm/Nd)_{source}$) [*DePaolo*, 1988] predicted under the same melting conditions as calculated for Th and U using analogous equations appropriate for modeling the behavior of stable elements [*Zou*, 1998]. In contrast to the short-lived U-series isotopes, fractionations of Sm and Nd are a function only of the overall melt fraction extracted and residual source porosity. Source lithologies are the same as in (A). Curves labeled "gt peridotite (SL)" and "gt pyroxenite (SL)" calculated using partition coefficients for garnet, cpx, and opx from the work of *Salters and Longhi* [1999] and for olivine from the work of *Dunn and Sen* [1994]. Curves labeled "gt pyroxenite (vW)" and "eclogite (vW)" calculated using partition coefficients of *van Westrenen et al.* [1999] for garnet and of *Lundstrom et al.* [1994] for clinopyroxene. Porosities used are 0.4% (gt peridotite (SL)), 1% (pyroxenite (SL)), 10.5% (pyroxenite (vW)), and 18% (eclogite (vW)). Also shown (right axis) are depleted mantle model ages for the source that correspond to a given $\alpha_{Sm/Nd}$, calculated using the depleted mantle Sm/Nd and ^{143}Nd/^{144}Nd of *Allègre et al.* [1983] and the Sm/Nd and ^{143}Nd/^{144}Nd ratios measured in the lavas. For example, if the AKB lavas represent a 4% partial melt of garnet peridotite, T_{DM} of the source would be ~1.3 Ga. All of these calculations assume steady state during dynamic partial melting; curves shown at low melt fractions before steady state is reached (<1–2%) may overestimate $\alpha_{Sm/Nd}$.

even lower porosities and/or melting rates than those shown. The presence of amphibole instead of phlogopite in the source would have similar effects.

[17] An important conclusion from the modeling presented above is that according to our current models for the behavior of U series nuclides during melting, with the exception of anhydrous melting of eclogite, it is quite difficult to produce melts with $(^{230}Th)/(^{238}U)$ as high as 1.36, even in the generous case of dynamic melting. If melt generation beneath Tibet is occurring by continuous melting (i.e., without significant upwelling), the required residual porosities and melting rates would be even smaller [*Williams and Gill*, 1989]. Conditions for genesis of the AKB lavas in the presence of eclogite are less restrictive than those for garnet peridotite, because of the combination of higher mineral-melt partition coefficients and modal percentage of garnet in eclogite. However, it is evident from the modeling presented above that both ultramafic and mafic lithologies are viable candidates for the source of the AKB lavas.

4.2. Evaluation of Possible Sources

4.2.1. Possible Source Lithologies

[18] The radiogenic Sr and Pb and unradiogenic Nd isotopic signatures of northern Tibetan magmas, including those of the AKB lavas, are features identified with ancient continental crust and with EMII-type mantle sources. EMII characteristics are recognized in peridotitic xenoliths derived from the subcontinental mantle lithosphere. They are also found in plume-derived OIBs but the isotopic compositions and high Th/U of the Ashikule magmas (Figure 2) are much more extreme than those of OIB [cf. *Zindler and Hart*, 1986]. Therefore, the more likely source for the AKB lavas is enriched lower crust or mantle that resides in the lithosphere rather than in the deep asthenosphere. Significantly, unlike the results for some basalts of the southwestern U.S. [e.g., *Asmerom*, 2000] but like those for basalts from northwestern China (Zou et al., in preparation), our data clearly show pronounced ^{230}Th excesses in rocks derived from lithospheric sources.

[19] The likely presence of garnet in the AKB source(s), including that in possible contaminants, precludes genesis of the AKB trachyandesites by partial melting of metasedimentary lower crustal rocks lacking garnet (for example, the xenoliths described by *Hacker et al.* [2000]). It does not however otherwise provide strict constraints on the location within the lithosphere of the source region, as garnet-bearing mafic or ultramafic rocks could reside in both the mantle and lower crust. Garnet pyroxenite and eclogite would plausibly be present in both the lower crust and mantle [e.g., *Hirschmann and Stolper*, 1996] and garnet peridotite would be present in the mantle at pressures >2.5 GPa (i.e., deeper than ~80 km). In particular, pyroxenite and/or eclogite veins or pods within an upper mantle dominated by peridotite would be a likely consequence of the accretion of tectonic blocks. Melting of such a mixed source [e.g., *Hirschmann and Stolper*, 1996; *Reiners*, 2002] would imply even lower porosities and/or melting rates than for garnet pyroxenite alone (cf. Figure 3), because melts of peridotite would have lower $(^{230}Th)/(^{238}U)$ than melts of the pyroxenite at similar conditions.

[20] By analogy to other alkaline volcanic rocks, the AKB trachyandesites likely represent differentiates of small-degree (3–5%) melts of an ultramafic source [e.g., *Williams et al.*, 1992; *Turner et al.*, 1996; *Miller et al.*, 1999; *Sims et al.*, 1999] or extracts of much larger-degree (20–50%) melting of a mafic source [e.g., *Sen and Dunn*, 1994; *Rapp and Watson*, 1995]. Experimental constraints on melting of metabasaltic compositions indicate that low to moderate-degree (<20–30%) melts are much more silicic than the AKB trachyandesites [e.g., *Sen and Dunn*, 1994; *Rapp and Watson*, 1995] but that larger-degree melting of amphibolites can produce liquids with silica contents similar to those of the AKB lavas (SiO_2 ~55–60%) in equilibrium with garnet eclogite residues. Available calculations and experimental data suggest that pyroxenite solidus temperatures and derivative melt compositions could vary widely depending on the bulk composition of the pyroxenite, and melts could include compositions that are broadly similar to the AKB lavas [*Hirschmann and Stolper*, 1996;

Hirschmann and Pertermann, 2000; *Pertermann and Hirschmann*, 2000].

[21] Dynamic experiments on mafic crustal lithologies [e.g., *Rushmer*, 1995] have shown that melts can be segregated in shear zones, such that even if melt fractions in excess of the critical melt fraction are not progressively removed, as formalized in the modeling above, stepwise extraction of ~5% crustal melts might be capable of producing U-Th disequilibria in the resulting aggregated melts. It is unclear, however, whether the duration of melting required at the melting rates permitted by the measured ^{230}Th excesses is sufficiently short so that appropriate volumes of melt (i.e., >25%) from eclogite could be aggregated. Durations of melting to produce 25% melt fractions of mafic sources range from 1.8 Ma (at 5×10^{-3} kg m^{-3} yr^{-1}) to 93 Ma (at 10^{-5} kg m^{-3} yr^{-1}); a magma reservoir of the limited size suggested by the small volume of erupted lavas in the AKB would be unlikely to remain both molten and undisturbed by tectonic events over these timescales. In contrast, 3–5% melting (of an ultramafic source) at those same rates would require a factor of ~10 less time. Continuous melting would imply slower melting and therefore even longer durations of melting, again underscoring the difficulty of producing high (^{230}Th)/(^{238}U) in the AKB lavas in the context of current melting models.

4.2.2. Nature and Timing of Source Enrichment

[22] The small degree of melting inferred for an origin of the AKB trachyandesites by melting of garnet peridotite or garnet pyroxenite would imply significantly higher concentrations of incompatible elements in the melts with respect to those in the source. Even if the trachyandesites are differentiates of more mafic magmas, the compositional difference between coexisting trachybasalts and trachyandesites in northwestern Tibet [*Arnaud et al.*, 1992] suggests that parental magmas may have trace element concentrations only a factor of 2 lower than those of the trachyandesites. Allowing for this, estimates for the concentrations of representative trace elements in various possible lithospheric lithologies can be calculated as a function of melt fractions; these are shown in Figure 4. Even at the smallest degrees of partial melting, the trace element characteristics inferred for the sources are enriched with respect to bulk Earth, qualitatively consistent with previous findings [*Turner et al.*, 1996]. However, our modeling indicates, in general, more fractionation of incompatible elements during melting than was assumed previously, permitting lower concentrations of incompatible elements in the source. Inferred source characteristics assuming $\leq$5% melt fractions of garnet peridotite are comparable to data for xenoliths and peridotite massifs (Figure 4). Inferred source concentrations assuming >10% melt fractions, on the other hand, are much higher than the values measured in most potential source analogs. The number of samples representative of corresponding lithologies are too few and too scattered to definitively distinguish the possible roles of different source lithologies. Calculated concentrations of U and Th for garnet pyroxenite and garnet peridotite sources (not shown) assuming melt fractions of $\geq$3% do not differ significantly and Th/U ratios of >4 are required in the mantle source for melt fractions of $\geq$1%. These calculations suggest that if the AKB lavas represent $\leq$5% partial melts of the mantle, the Tibetan mantle lithosphere could contain similar abundances of incompatible trace elements as do xenoliths and massifs.

[23] Even though the source of the AKB lavas is not required to have unusually elevated concentrations of incompatible trace elements, the isotopic characteristics of the lavas are those of an enriched source. In the case of the mantle, this could be a mixed pyroxenite-peridotite source. Other potential agents for mantle enrichment are hydrous and carbonic fluids. The observed enrichments of ^{230}Th relative to ^{238}U are uncharacteristic of melts produced by fluxing the mantle with such fluids, as the incorporation of (typically U-enriched) hydrous fluids during melting has been inferred to be the cause of the U enrichments found in many arc lavas [e.g., *Gill and Williams*, 1990; *Condomines and Sigmarsson*, 1993; *Chabaux and Allegre*, 1994]. On the other hand, ancient metasomatic phases precipitated in mantle rocks from hydrous or carbonic fluids may have contributed to the melts [cf.

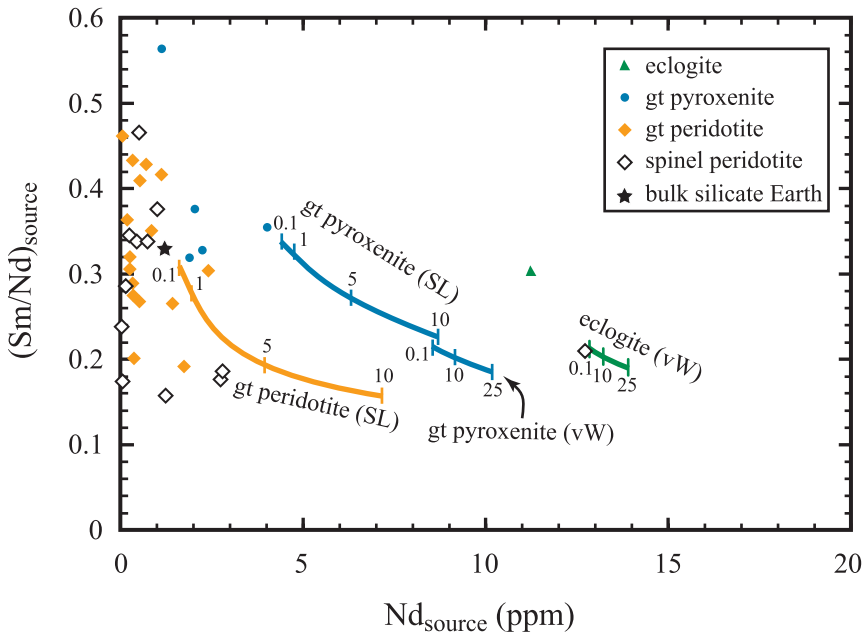

Figure 4. Curves illustrate Sm/Nd ratios and Nd concentrations in potential source rocks that would be in equilibrium with melts parental to the AKB lavas if produced during dynamic melting under the same conditions as in Figure 3. Tick marks along curves are labeled with melt fractions extracted (in %). In the case of garnet peridotite, where primary liquids are likely to have been more mafic than those erupted, concentrations of Sm and Nd in the primary liquid were assumed to be a factor of 2 lower than those measured in the erupted liquids. In the case of eclogite, where the erupted compositions could potentially represent primitive melts, concentrations measured in AKB-1 were used to calculate source concentrations. Two possibilities are presented in the case of pyroxenite melts: small-degree melts of pyroxenite using partition coefficients of *Salters and Longhi* [1999] and *Dunn and Sen* [1994] (SL) were assumed to have concentrations a factor of 2 lower than erupted lavas, whereas large-degree melts of garnet pyroxenite using partition coefficients of *van Westrenen et al.* [1999] and *Lundstrom et al.* [1994] (vW) were assumed to have concentrations like those in erupted lavas. Also shown are values measured in mantle xenoliths and peridotite massifs [*McDonough*, 1990; *Tatsumoto et al.*, 1992; *Becker*, 1993, 1996; *Qi et al.*, 1995; *Hirschmann and Stolper*, 1996; *Mukasa and Wilshire*, 1997] and an estimate for bulk silicate Earth [*McDonough and Sun*, 1995]. All of these calculations assume steady state during dynamic partial melting; curves at low melt fractions (<2%) may underestimate the degree of fractionation of Sm from Nd and therefore underestimate Sm/Nd in the source. See text for discussion. Data used to construct this diagram are available in the auxiliary material.

Turner et al., 1996] but, as discussed above, partial melts of a phlogopite- or amphibole-bearing source would have smaller ^{230}Th excesses than would partial melts of a similar but anhydrous source. Alternatively, if precipitated not long (<∼200 ka) before melting, metasomatic phases could have $(^{230}Th)/(^{238}U) \gg 1$ (e.g., $D_{Th}/D_U = 2.6$ has been measured for amphibole in equilibrium with hydrous fluid) [*Brenan et al.*, 1995]. In order for metasomatic phases to have contributed to the high $(^{230}Th)/(^{238}U)$ signatures of the AKB lavas, they must have had high concentrations of Th and U relative to the anhydrous phases and/or have melted preferentially such that they dominated the Th and U budget of the resulting melts. Unlike the Gaussberg lamproites, however, for which large ^{230}Th enrichments have been attributed to disequilibrium melting of phlogopite [*Williams et al.*, 1992], the bulk compositions of the Ashikule magmas are not those expected of a melting mode dominated by metasomatic phases. It appears therefore that, if present, hydrous metasomatic phases must constitute a relatively small proportion of the source of the AKB lavas, suggesting that the main metasomatizing agent was relatively dry silicate melt.

[24] *Turner et al.* [1996] obtained an age of >1.2 Ga for the source based on Nd and Pb isotope signatures. Such inferences are critically dependent on the source lithology, melting process, and total

melt fraction since these dictate the magnitude of melting related Sm/Nd fractionation. As is illustrated in Figure 3C, $\alpha_{Sm/Nd}$ values (Sm/Nd ratio of the melt normalized to the Sm/Nd ratio of the source [*DePaolo*, 1988]) could range from ~0.4 to ~0.75 for garnet peridotite or pyroxenite sources and melt fractions of 3–5%, or from ~0.65 to 0.75 for larger degrees of melting of eclogitic or pyroxenitic sources. Based on this, the minimum duration of source enrichment is ~1 Ga, if the lithology of the source is a peridotite (Figure 3C), but could be much older for smaller-degree melting of a garnet peridotite or garnet pyroxenite source. For such ancient enrichments, a time-integrated Th/U of ~4.1 can explain the Pb isotope signatures. Even allowing for the possibility of ^{230}Th enrichment due to ingrowth during melting, the low (^{230}Th)/(^{232}Th) ratios measured in AKB lavas correspond to present-day ^{232}Th/^{238}U ratios in their source(s) of ≥4.5 (Figure 2). The fact that the two estimates of Th/U are different could reflect decay of ^{230}Th during magma transport and differentiation or could be the product of a multistage history of lithospheric accretion and/or mantle enrichment. In the extreme case, enrichment could have occurred by silicate melts derived from sources foreign to the lithospheric domain in which they now reside, in which case neither the enriched Nd or Pb isotope signatures would necessarily be longstanding features of the source region.

5. Additional Considerations

[25] The trace element and isotopic data discussed above indicate that the source of the AKB magmas is a garnet-bearing mafic to ultramafic assemblage that has probably been enriched in incompatible elements relative to bulk Earth since at least the middle Proterozoic (>1 Ga). This combination of characteristics suggests that the magma source region most likely resides within the lithosphere. In this section, we consider how these characteristics, together with the melting rates inferred from the U-Th disequilibria, may provide constraints on the tectonic setting(s) of melt generation and whether they have bearing on the interpretation of geophysical observations within the crust.

5.1. Implications for the Nature of Midcrustal Fluid

[26] Various geophysical observations suggest the presence, at least locally, of a fluid in the Tibetan middle to lower crust. The fluid has been interpreted as a partial melt in the northern Tibetan Plateau [*Owens and Zandt*, 1997; *Wei et al.*, 2001], and as either a partial melt [*Nelson et al.*, 1996] or a saline brine fluid [*Wei et al.*, 2001] or both [*Makovsky and Klemperer*, 1999] in southern Tibet. Assuming that inferences about melting process and source based on the AKB data can be generalized to the widespread, chemically similar mafic volcanic rocks of northern Tibet, the following observations are pertinent: (1) silicic volcanic rocks like those expected from crustal melting are not common in northern Tibet [e.g., *Deng*, 1993; *Turner et al.*, 1996], (2) widespread pooling of crustal melts (such as would be necessary to explain the geophysical observations) would likely inhibit the passage of the mafic magmas that are more common eruptive products in northern Tibet, and (3) whereas the postulated fluids could represent midcrustal pooling of mafic melts derived from deeper crustal or mantle sources, by analogy to the AKB magmas residence times in the crust are unlikely to be more than tens of thousands of years based on the transient nature of large ^{230}Th excesses. Just as for the volcanic rocks, the distribution of fluids is geographically widespread but localized, so that it is difficult to explicitly test the relationship between the two.

5.2. Tectonic Setting of Melt Generation

[27] The geochemical characteristics of Tibetan magmas place constraints on models proposed to explain melt generation in the tectonic context of the Tibetan plateau. In particular, as argued above, the Th isotope data indicate that the role of hydrous metasomatic fluids or hydrous phases in melt production is probably limited. Therefore, melting due to fluid release during intracontinental subduction [e.g., *Arnaud et al.*, 1992; *Tapponnier et al.*, 2001] seems unlikely. Moreover, subduction of the Tarim basin beneath the Tibetan plateau [*Lyon-Caen and Molnar*, 1984] would likely occur at a relatively

shallow angle, and thus the position of the AKB, ~120 km behind the "trench" (as inferred from the thickest sediment cover in the Tarim basement to the north [*Cowgill*, 2001]), is likely to be above a relatively shallow part of the downgoing slab, where pressures and temperatures are likely too low for dehydration of hydrous upper-crustal assemblages to occur.

[28] One alternative mechanism for inducing melting in the upper mantle lithosphere or lowermost crust is heating through viscous dissipation, as presented by *Kincaid and Silver* [1996]. Although their modeling suggests that it is unlikely that the lower crust or upper mantle would reach temperatures corresponding to the dry peridotite solidus, temperatures could be above the wet peridotite solidus or, by extension, the pyroxenite solidus [cf. *Hirschmann and Stolper*, 1996]. Partial melting of mafic (eclogitic or pyroxenitic) assemblages could, as discussed above, account for the ^{230}Th-^{238}U disequilibria measured in the AKB samples. Besides mafic lower crust, it is plausible that pyroxenite veins or pods present within the lithospheric mantle could be a source of melts through this mechanism, and would be expected given evidence for ancient and/or multiple enrichment events in the Tibetan source.

[29] A commonly proposed mechanism for producing melts in the lithospheric mantle is juxtaposition of hot asthenosphere against the remaining (upper) mantle lithosphere following convective erosion of the thickened lower lithospheric mantle [*Molnar et al.*, 1993; *Turner et al.*, 1996]. Studies of shear wave splitting in the upper mantle beneath northern Tibet suggest that the lithospheric mantle can not have been completely removed [*Lave et al.*, 1996; *Silver*, 1996; *Holt*, 2000], consistent with derivation of magmas from an ancient, enriched lithospheric source suggested by our and previous workers' geochemical data [e.g., *Arnaud et al.*, 1992; *Turner et al.*, 1996]. Recent work incorporating a temperature-dependent viscosity of the mantle suggests that removal of lithospheric mantle may be delayed with respect to the onset of thickening, which may be problematic when considering the mechanism for producing early Tibetan volcanism but not for the genesis of the relatively recent volcanism on the Tibetan plateau [*Lenardic and Kaula*, 1995; *Conrad*, 2000]. In this case, as well as the previous cases, melting would be primarily the result of heat input, and therefore residual porosities and melting rates obtained from the dynamic melting modeling presented above would be maxima. Nevertheless, the maximum melting rates obtained from dynamic melting models could potentially be coupled with modeling of the rates of temperature increase expected during convective removal to provide a test of this model.

[30] A striking feature of the distribution of volcanic rocks in northern and central Tibet, and one that is not explicitly addressed by existing models, is that they are spatially associated with strike-slip faults. Moreover, the same relationship has been noted for potassic volcanic rocks associated with the North Anatolian Fault in Turkey [*Adiyaman et al.*, 2001] which are also enriched in incompatible trace elements (although to a somewhat lesser degree than the Tibetan lavas). The relationship may simply be passive if the faults are conduits for magma transport to the surface. When coupled with the geophysical support for coherence between surface deformation and deformation at depth [*Lave et al.*, 1996; *Wittlinger et al.*, 1998; *Holt*, 2000] and geochemical evidence that the lavas may be small melt fractions, however, this spatial association of magmatism and faulting warrants consideration of a fault-related mechanism for melting itself [*Yin et al.*, 1995]. Even a small amount of mantle upwelling and attendant decompression produced by thinning of the lithosphere in releasing bends along strike-slip faults [*Yin et al.*, 1995] could potentially induce small degrees of partial melting, if the mantle was at or near its solidus prior to extension (as may be the case if the lithospheric mantle was metasomatized and then thickened and heated).

[31] In order to assess whether lithospheric thinning across a releasing bend in a strike-slip fault could produce melts with U-Th disequilibria like those of the AKB lavas, we modeled melting associated with pure-shear lithospheric deformation produced by such extension. The results of

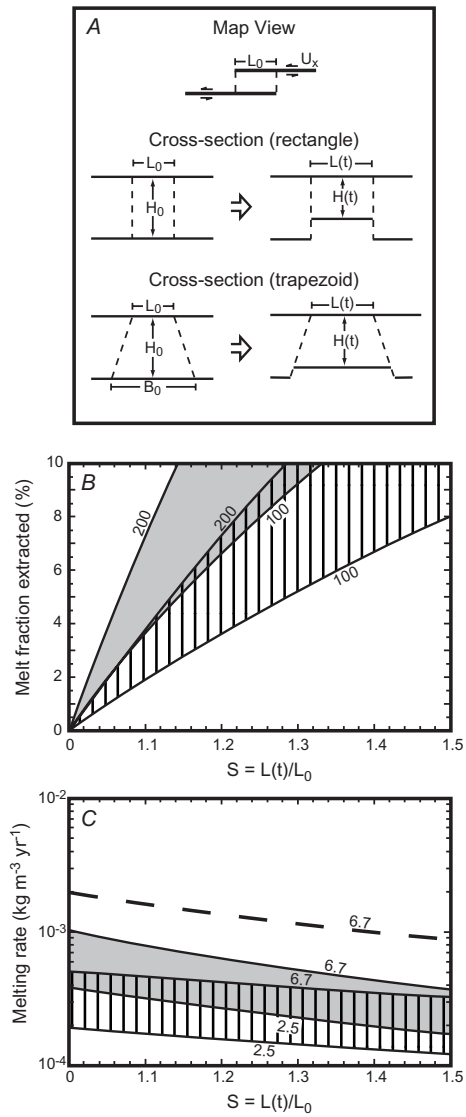

Figure 5. (A) Sketch illustrating relationship between model parameters. Assuming an initial step in a strike-slip system of length L_0 (map view sketch), dashed lines enclose the surface area affected by extension. Cross sections show geometry of extended and uplifted areas in the case where all extension at the surface is transmitted vertically downward (rectangle) or where the extension affects a broader area at depth than at the surface (trapezoid). See text and Appendix A for discussion. (B) Melt fraction extracted (in %) related to surface extension (S). S is the stretch or degree of extension, defined as the length of the offset at time t after initiation of extension (Lt) relative to the initial length (L_0): $S = L_t/L_0 = 1 + (tU_x/L_0)$ [cf. *Leeman and Harry*, 1993]. Shaded field indicates models with rectangular geometry and ruled area indicates trapezoidal geometry. Numbers next to lower and upper bounds on fields indicate initial lithospheric thickness (in km). (C) Melting rate versus extension. The melting rate relative to degree of extension is a function of the melt productivity, the initial aspect ratio of the lithospheric section (z_0/L_0), and the extension rate (see Appendix A), assuming a negligible change in solid density (ρ_s) due to upwelling. Fields as in (B). All models shown assume slip rate of 12 mm yr^{-1}, with the exception of the dashed line (slip rate 23 mm yr^{-1}). Numbers next to lower and upper bounds on fields indicate z_0/L_0, from 6.7 (e.g., z_0 = 200 km and L_0 = 30 km) to 2.5 (e.g., z_0 = 100 km and L_0 = 40 km). Model parameters in (B) and (C) are estimated from the following sources: Lithospheric thickness of 100–200 km [e.g., *Brandon and Romanowicz*, 1986; *Holt and Wallace*, 1990; *Silver*, 1996; *Owens and Zandt*, 1997], slip rates on the Altyn Tagh fault of 12–23 mm yr^{-1} [*Ryerson et al.*, 1999], and melt productivity during adiabatic decompression of 0.4% km^{-1} [e.g., *Langmuir et al.*, 1992]. Increasing the slip rate will increase both melting rate and degree of melting (see equations (1), (2), (3), and (4) in Appendix A). Decreasing productivity to 0.1% (a likely minimum) [*Hirschmann and Stolper*, 1996] will decrease both melting rate and degree of melting (see (C)) by a factor of 4.

this simple model are illustrated in Figure 5, and the model is explained more fully in Appendix A. Melting parameters obtained from the dynamic melting modeling presented above would be directly applicable in this case. Other variables controlling lithospheric thinning and melt production are not well known but we can delimit the likely range of melting rate and total melt produced by considering a reasonable range of values for melt productivity, the initial aspect ratio of the lithospheric section (z_0/L_0) and the extension rate (see Figure 5). Ratios of initial surface length to length at depth of 1 (rectangular geometry) to 3 (trapezoidal geometry; see Figure 5A) were used because recent tomographic evidence suggests that the Altyn Tagh fault near the Qaidam Basin extends as a shear zone to at least 140 km depth [*Wittlinger et al.*, 1998], and shear wave anisotropy in the mantle shows a correlation with surface structures, implying that the lithosphere is vertically coherent during deformation [*Lave et al.*, 1996; *Wittlinger et al.*, 1998; *Holt*, 2000]. Diffusive heat loss from the source rock is assumed to be slow relative to advective transport. Using this range of parameters, <30% extension across a releasing bend in a strike-slip fault (S < 1.3) is capable of producing the 3–5% melt fractions consistent with the bulk composition of Ashikule magmas and corresponds to melting rates of approximately 1×10^{-4} to 2×10^{-3} kg m^{-3} yr^{-1}. This range of melting rates overlaps the range (albeit at the high end) of the maximum melting rates consistent with the Th enrichments measured in the AKB lavas.

[32] In summary, a number of mechanisms could potentially produce the small-degree melts erupted as the AKB and other Tibetan lavas, as long as the lower-crustal or mantle source is near its solidus. Given the scale and complexity of the Indo-Asian collision, it would not be surprising if the different melting mechanisms proposed for volcanic rocks of northern Tibet are operating simultaneously across the plateau, or even at different depths within the lithosphere beneath one region. An important implication of a diversity of permissible melting mechanisms, including the possibility of fault-related melting, would be that the magmatism need not be directly related to lithospheric thickening or mantle delamination and therefore to uplift of the plateau.

6. Summary

1. Potassic trachyandesite and trachybasalt lavas in the AKB of northwestern Tibet are characterized by excesses of ^{230}Th relative to ^{238}U, up to a maximum (^{230}Th)/(^{238}U) of 1.36, by large enrichments in incompatible trace elements compared to bulk Earth values, and by radiogenic Sr and Pb isotope ratios and unradiogenic Nd isotope ratios. These geochemical characteristics are similar to other Tibetan volcanic rocks, and therefore mechanisms of melt generation that can account for the AKB lavas may exemplify those for other Tibetan lavas.

2. ^{230}Th excesses of the magnitude observed for the AKB lavas are unlikely to be produced during differentiation of a magma, instead reflecting partial melting of mantle or crustal assemblages. Modeling of dynamic melting indicates that partial melting of a garnet-bearing source is required in order to produce (^{230}Th)/(^{238}U) $\geq$ 1.36. Small porosities (<0.4%) and slow melting rates ($<10^{-4}$ kg m^{-3} yr^{-1}) are required in the case of a garnet peridotite residue, although larger porosity (up to 18%) and melting rates ($>10^{-3}$ kg m^{-3} yr^{-1}) are permitted in the case of an eclogitic residue.

3. Potential source lithologies could plausibly reside either in the mantle or in the crust. To be consistent with melting constraints inferred from the ^{230}Th excesses, concentrations of incompatible elements in the source may be somewhat higher than bulk Earth, but could be similar to those measured in xenoliths and peridotite massifs. Unless the Nd, Pb, and Th isotopic characteristics of the AKB magmas reflect metasomatism of the lithosphere by silicate melts derived from other sources, the source of the melts has been enriched in incompatible elements with respect to bulk Earth since at least the middle Proterozoic (>1 Ga), and may have experienced a multistage enrichment history.

4. A number of mechanisms could potentially account for the geochemical characteristics of the AKB magmas, including shear heating during deformation, convective removal of the lowermost lithospheric mantle and heating of the remaining lithosphere, or upwelling associated with extension

along releasing bends in strike-slip faults. Melting due to fluid release during intracontinental subduction is, however, inconsistent with the geochemical data.

Appendix A

[33] For a vertical lithospheric section of initial thickness z_0 undergoing pure-shear thinning due to horizontal extension (Figure 5) the mass fraction of melt (F) produced during uplift of the base of the lithosphere will be given by

$$F = \left(\frac{dF}{dz}\right)\Delta z = \left(\frac{dF}{dH}\right)\left[z_0 - \frac{z_0}{S}\right] \quad (1)$$

where (dF/dz) is the melt productivity (%/km) and S is the stretch or degree of extension, defined as the length of the offset at time t after initiation of extension (L_t) relative to that initially (L_0): $S = L_t/L_0 = 1 + (tU_x/L_0)$ [cf. *Leeman and Harry*, 1993]. The rate of extension (U_x) is assumed to be constant, and for offsets of parallel fault segments, is equal to the slip rate. For a given value of S, melt fraction is therefore only a function of the initial lithospheric thickness. Assuming that all thinning is expressed as uplift at the base of the lithosphere (i.e., no isostatic compensation; including Airy isostasy in the equations makes virtually no difference in the calculated melt fractions or melting rates), the melting rate dF/dt (kg m^{-3} yr^{-1}) is a function of the rate of uplift, dz/dt, and can be expressed as

$$\frac{dF}{dt} = \left(\frac{dz}{dt}\right)\left(\frac{dF}{dz}\right)\rho_s = \left[\frac{z_0 U_x}{L_0 S^2}\right]\left(\frac{dF}{dz}\right)\rho_s \quad (2)$$

The simple geometry of the foregoing discussion assumes that the lithosphere behaves as a vertically coherent block, in keeping with the observations of recent work [*Lave et al.*, 1996; *Wittlinger et al.*, 1998; *Holt*, 2000]. In addition, it implicitly assumes that deformation at depth is confined entirely to a vertical column below the surface expression of the fault. Relaxing these conditions poses a problem that is beyond the scope of this paper, the full treatment of which, given the present uncertainties in the parameters of the model, is not likely to lead to significantly better constraints on the conditions of melting. Nevertheless, the qualitative behavior of the system as described above is likely to be robust. To illustrate this, we examine the effect that a trapezoidal geometry, representing broadening of the deformation zone at depth, may have on the rates of uplift at the base of the lithosphere and therefore on the melting dynamics. The expressions analogous to equations (1) and (2) for a trapezoid are:

$$F = \left(\frac{dF}{dz}\right)\Delta z = \left(\frac{dF}{dz}\right)\left[z_0 - \frac{z_0\left(\frac{1+C}{2}\right)}{S + \left(\frac{C-1}{2}\right)}\right] \quad (3)$$

$$\frac{dF}{dt} = \left(\frac{dF}{dz}\right)\left(\frac{dz}{dt}\right)\rho_s = \left(\frac{dF}{dz}\right)\left[\frac{z_0 U_x\left(\frac{1+C}{2}\right)}{L_0\left(S + \left(\frac{C-1}{2}\right)\right)^2}\right]\rho_s \quad (4)$$

where C is a constant relating the initial length of the top and base of the trapezoid such that the length of the base $B_0 = CL_0$ (see Figure 5A). The value of C depends on the rheology of the mantle and is a measure of how efficiently the surface extension is transmitted through the mantle at depth. As could be anticipated, the qualitative effect of allowing the area affected by deformation at depth to be larger than that at the surface will be to decrease the uplift and therefore the degree of melting as well as the melting rate for a given degree of surface extension (Figure 5).

Acknowledgments

[34] Support of NSF EAR9418323 and EAR9980646 to MRR is gratefully acknowledged. The writing of this paper was partially supported by a NSF Graduate Research Fellowship and a UC Office of the President Dissertation-Year Fellowship to KMC. A Sigma Xi research grant to KMC provided partial funding for fieldwork in the Pulu area in 1996. KMC thanks Caltech for a geochemistry option postdoctoral fellowship during the final stages of revision of the manuscript. We thank F. Ramos for running the Pb isotope analyses presented here. We would like to thank A. Yin for encouraging the development of the model for extension-related melting and E. Cowgill for his insights about the structural setting of volcanism, for allowing us to use his geologic map of the AKB area, and for help in obtaining and interpreting the ASTER data. Thanks to K. Sims, H. Zou, and the Asian Tectonics group at UCLA for discussions about various aspects of this project. Earlier versions of this manuscript benefited from comments by T. LaTourrette, A. Yin, and T. M. Harrison. Constructive and thorough reviews by P. Reiners and S. Turner and comments and editorial handling

by R. Rudnick and W. White led to substantial improvements in the manuscript.

References

Adiyaman, O., J. Chorowicz, O. N. Arnaud, M. N. Gundogdu, and A. Gourgaud, Late Cenozoic tectonics and volcanism along the North Anatolian Fault: New structural and geochemical data, *Tectonophysics*, *338*, 135–165, 2001.

Allègre, C. J., S. R. Hart, and J.-F. Minster, Chemical structure and evolution of the mantle and continents determined by inversion of Nd and Sr isotopic data, I, Theoretical models, *Earth Planet. Sci. Lett.*, *66*, 177–190, 1983.

Arnaud, N. O., P. Vidal, P. Tapponnier, P. Matte, and W. M. Deng, The high K_2O volcanism of northwestern Tibet: Geochemistry and tectonic implications, *Earth Planet. Sci. Lett.*, *111*, 351–367, 1992.

Asmerom, Y., Th-U fractionation and mantle structure, *Earth Planet. Sci. Lett.*, *166*, 163–175, 1999.

Asmerom, Y., Melting of the Earth's lithospheric mantle inferred from protactinium–thorium–uranium isotopic data, *Nature*, *406*, 293–296, 2000.

Asmerom, Y., and R. L. Edwards, U-series isotope evidence for the origin of continental basalts, *Earth Planet. Sci. Lett.*, *134*, 1–7, 1995.

Beattie, P., Uranium–thorium disequilibria and partitioning on melting of garnet peridotite, *Nature*, *363*, 63–65, 1993.

Becker, H., Garnet peridotite and eclogite Sm-Nd mineral ages from the Lepontine dome (Swiss Alps): New evidence for Eocene high-pressure metamorphism in the central Alps, *Geology*, *21*, 599–602, 1993.

Becker, H., Geochemistry of garnet peridotite massifs from lower Austria and the composition of deep lithosphere beneath a Palaeozoic convergent plate margin, *Chem. Geol.*, *134*, 49–65, 1996.

Bourdon, B., C. H. Langmuir, and A. Zindler, Ridge–hotspot interaction along the Mid-Atlantic Ridge between 37°30′ and 40°30′N: The U-Th disequilibrium evidence, *Earth Planet. Sci. Lett.*, *142*, 175–189, 1996a.

Bourdon, B., A. Zindler, T. Elliott, and C. H. Langmuir, Constraints on mantle melting at mid-ocean ridges from global ^{238}U-^{230}Th disequilibrium data, *Nature*, *384*, 231–235, 1996b.

Bourdon, B., S. J. Goldstein, D. Bourlès, M. T. Murrell, and C. H. Langmuir, Evidence from ^{10}Be and U series disequilibria on the possible contamination of mid-ocean ridge basalt glasses by sedimentary material, *Geochem. Geophys. Geosyst.*, *1*, 10.1029/2000GC000047, 2000.

Brandon, C., and B. Romanowicz, A "No-lid" zone in the central Chang-Thang platform of Tibet: Evidence from pure path phase velocity measurements of long-period Rayleigh waves, *J. Geophys. Res.*, *91*, 6547–6564, 1986.

Brenan, J. M., H. F. Shaw, F. J. Ryerson, and D. L. Phinney, Mineral-aqueous fluid partitioning of trace elements at 900°C and 2.0 GPa: Constraints on the trace element chemistry of mantle and deep crustal fluids, *Geochim. Cosmochim. Acta*, *59*, 3331–3350, 1995.

Chabaux, F., and C. Allègre, ^{238}U-^{230}Th-^{226}Ra disequilibria in volcanics: A new insight into melting conditions, *Earth Planet. Sci. Lett.*, *126*, 61–74, 1994.

Chabaux, F., C. Hemond, and C. J. Allègre, ^{238}U-^{230}Th-^{226}Ra disequilibria in the Lesser Antilles arc: Implications for mantle metasomatism, *Chem. Geol.*, *153*, 171–185, 1999.

Clark, S. K., M. K. Reagan, and T. Plank, Trace element and U-series systematics for 1963–1965 tephras from Irazu Volcano, Costa Rica: Implications for magma generation processes and transit times, *Geochim. Cosmochim. Acta*, *62*, 2689–2699, 1998.

Claude-Ivanaj, C., B. Bourdon, and C. Allègre, Ra-Th-Sr isotope systematics in Grande Comore Island: A case study of plume–lithosphere interaction, *Earth Planet. Sci. Lett.*, *1998*, 99–117, 1998.

Cohen, A. S., R. K. O'Nions, and M. D. Kurz, Chemical and isotopic variations in Mauna Loa tholeiites, *Earth Planet. Sci. Lett.*, *143*, 111–124, 1996.

Condomines, M., and O. Sigmarsson, Why are so many arc magmas close to ^{238}U-^{230}Th radioactive equilibrium?, *Geochim. Cosmochim. Acta*, *57*, 4491–4497, 1993.

Condomines, M., J.-C. Tanguy, and V. Michaud, Magma dynamics at Mt. Etna: Constraints from U-Th-Ra-Pb radioactive disequilibria and Sr isotopes in historical lavas, *Earth Planet. Sci. Lett.*, *132*, 25–41, 1995.

Conrad, C. P., Convective instability of thickening mantle lithosphere, *Geophys. J. Int.*, *143*, 52–70, 2000.

Cooper, K. M., M. R. Reid, M. T. Murrell, and D. A. Clague, Crystal and magma residence at Kilauea Volcano, Hawaii: ^{230}Th-^{226}Ra dating of the 1955 east rift eruption, *Earth Planet. Sci. Lett.*, *184*, 703–718, 2001.

Coulon, C., H. Maluski, C. Bollinger, and S. Wang, Mesozoic and Cenozoic volcanic rocks from central and southern Tibet: $^{40}Ar/^{39}Ar$ dating, petrological characteristics and geodynamical significance, *Earth Planet. Sci. Lett.*, *79*, 281–302, 1986.

Cowgill, E. S., Tectonic evolution of the Altyn Tagh-Western Kunlun Fault System, Northwestern China, Ph.D. thesis, Univ. of Calif. Los Angeles, Los Angeles, Calif., 2001.

Deng, W., Study on trace element and Sr, Nd isotopic geochemistry of Cenozoic potassic volcanic rocks in north Tibet, *Acta Petrol. Sin.*, *9*(4), 379–387, 1993.

Deng, W., *Cenozoic Intraplate Volcanic Rocks in the Northern Qinghai-Xizang Plateau*, 180 pp., Geol. Publ. House, Beijing, 1998.

DePaolo, D. J., *Neodymium Isotope Geochemistry*, Springer-Verlag, New York, 1988.

Dewey, J. F., R. M. Shackleton, C. Chang, and Y. Sun, The tectonic evolution of the Tibetan Plateau, *Philos. Trans. R. Soc. London, Ser. A*, *327*, 379–413, 1988.

Dunbar, N. W., W. C. McIntosh, and F. M. Phillips, Field relationships, chronology and petrology of a volcanic system in the Northern Tibetan Plateau, *Eos Trans. AGU*, S292, 1996.

Dunn, T., and C. Sen, Mineral/matrix partition coefficients for orthopyroxene, plagioclase, and olivine in basaltic to andesitic systems: A combined analytical and experimental study, *Geochim. Cosmochim. Acta*, *58*, 717–733, 1994.

Elliott, T., Fractionation of U and Th during mantle melting: A reprise, *Chem. Geol.*, *139*, 165–183, 1997.

Gauthier, P.-J., and M. Condomines, ^{210}Pb-^{226}Ra radioactive disequilibria in recent lavas and radon degassing: Inferences on the magma chamber dynamics at Stromboli and Merapi volcanoes, *Earth Planet. Sci. Lett.*, *172*, 111–126, 1999.

Gill, J. B., and R. W. Williams, Th isotope and U-series studies of subduction-related volcanic rocks, *Geochim. Cosmochim. Acta*, *54*, 1427–1442, 1990.

Gill, J. B., J. D. Morris, and R. W. Johnson, Timescale for producing the geochemical signature of island arc magmas: U-Th-Po and Be-B systematics in recent Papua New Guinea lavas, *Geochim. Cosmochim. Acta*, *57*, 4269–4283, 1993.

Goldstein, S. J., M. T. Murrell, and D. R. Janecky, Th and U isotopic systematics of basalts from the Juan de Fuca and Gorda Ridges by mass spectrometry, *Earth Planet. Sci. Lett.*, *96*, 134–146, 1989.

Goldstein, S. J., M. T. Murrell, D. R. Janecky, J. R. Delaney, and D. A. Clague, Geochronology and petrogenesis of MORB from the Juan de Fuca and Gorda Ridges by ^{238}U-^{230}Th disequilibrium, *Earth Planet. Sci. Lett.*, *107*, 25–41, 1991.

Goldstein, S. J., M. T. Murrell, and R. W. Williams, ^{231}Pa and ^{230}Th chronology of mid-ocean ridge basalts, *Earth Planet. Sci. Lett.*, *115*, 151–159, 1993.

Hacker, B. R., E. Gnos, L. Ratsbacher, M. Grove, M. McWilliams, S. V. Sobolev, W. Jiang, and Z. Wu, Hot and dry deep crustal xenoliths from Tibet, *Science*, *287*, 2463–2466, 2000.

Hauri, E. H., T. P. Wagner, and T. L. Grove, Experimental and natural partitioning of Th, U, Pb and other trace elements between garnet, clinopyroxene and basaltic melts, *Chem. Geol.*, *117*, 149–166, 1994.

Hirschmann, M., and M. Pertermann, Application of MELTS to pyroxenite partial melting in basalt source regions, in *Tenth Annual Goldschmidt Conference*, pp. 519, Cambridge Publ., Oxford, UK, 2000.

Hirschmann, M. M., and E. M. Stolper, A possible role for garnet pyroxenite in the origin of the "garnet signature" in MORB, *Contrib. Mineral. Petrol.*, *124*, 185–208, 1996.

Holt, W. E., Correlated crust and mantle strain fields in Tibet, *Geology*, *28*, 67–70, 2000.

Holt, W. E., and T. C. Wallace, Crustal thickness and upper mantle velocities in the Tibetan plateau region from the inversion of regional Pnl waveforms: Evidence for a thick upper mantle lid beneath southern Tibet, *J. Geophys. Res.*, *95*, 12,499–12,525, 1990.

Huang, Y., C. Hawkesworth, P. van Calsteren, I. Smith, and P. Black, Melt generation models for the Auckland volcanic field, New Zealand: Constraints from U-Th isotopes, *Earth Planet. Sci. Lett.*, *149*, 67–84, 1997.

Kincaid, C., and P. Silver, The role of viscous dissipation in the orogenic process, *Earth Planet. Sci. Lett.*, *142*, 271–288, 1996.

Kosarev, G., R. Kind, S. V. Sobolev, X. Yuan, W. Hanka, and S. Oreshin, Seismic evidence for a detached Indian lithospheric mantle beneath Tibet, *Science*, *283*, 1306–1309, 1999.

Landwehr, D., J. Blundy, E. M. Chamorro-Perez, E. Hill, and B. Wood, U-series disequilibria generated by partial melting of spinel lherzolite, *Earth Planet. Sci. Lett.*, *188*, 329–348, 2001.

Langmuir, C. H., E. M. Klein, and T. Plank, Petrological systematics of mid-ocean ridge basalts: Constraints on melt generation beneath ocean ridges, in *Mantle Flow and Melt Generation at Mid-Ocean Ridges*, edited by J. P. Morgan et al., p. 361, AGU, Washington, D. C., 1992.

LaTourrette, T., R. L. Hervig, and J. R. Holloway, Trace element partitioning between amphibole, phlogopite, and basanite melt, *Earth Planet. Sci. Lett.*, *135*, 13–30, 1995.

LaTourrette, T. Z., and D. S. Burnett, Experimental determination of U and Th partitioning between clinopyroxene and natural and synthetic basaltic liquid, *Earth Planet. Sci. Lett.*, *110*, 227–244, 1992.

LaTourrette, T. Z., A. K. Kennedy, and G. J. Wasserburg, Thorium–radium fractionation by garnet: Evidence for a deep source and rapid rise of oceanic basalts, *Science*, *261*, 739–742, 1993.

Lave, J., J. P. Avouac, R. Lacassin, P. Tapponnier, and J. P. Montagner, Seismic anisotropy beneath Tibet: Evidence for eastward extrusion of the Tibetan lithosphere?, *Earth Planet. Sci. Lett.*, *140*, 83–96, 1996.

Leeman, W. P., and D. L. Harry, A binary source model for extension-related magmatism in the Great Basin, western North America, *Science*, *262*, 1550–1554, 1993.

Lenardic, A., and W. M. Kaula, More thoughts on convergent crustal plateau formation and mantle dynamics with regard to Tibet, *J. Geophys. Res.*, *100*, 15,193–15,203, 1995.

Lundstrom, C. C., H. F. Shaw, F. J. Ryerson, D. L. Phinney, J. B. Gill, and Q. Williams, Compositional controls on the partitioning of U, Th, Ba, Pb, Sr, and Zr between clinopyroxene and haplobasaltic melts: Implications for uranium series disequilibria in basalts, *Earth Planet. Sci. Lett.*, *128*, 407–423, 1994.

Lundstrom, C. C., J. Gill, Q. Williams, and M. R. Perfit, Mantle melting and basalt extraction by equilibrium porous flow, *Science*, *270*, 1958–1961, 1995.

Lundstrom, C. C., D. E. Sampson, M. R. Perfit, J. B. Gill, and Q. Williams, Insights into mid-ocean ridge basalt petrogenesis: U-series disequilibria from the Siqueiros Transform, Lamont Seamounts, and the East Pacific Rise, *J. Geophys. Res.*, *104*, 13,035–13,048, 1999.

Lyon-Caen, H., and P. Molnar, Gravity anomalies and the structure of western Tibet and the southern Tarim basin, *Geophys. Res. Lett.*, *11*(12), 1251–1254, 1984.

Makovsky, Y., and S. L. Klemperer, Measuring the seismic properties of Tibetan bright spots: Evidence for free aqueous fluids in the Tibetan middle crust, *J. Geophys. Res.*, *104*, 10,795–10,825, 1999.

Matte, P., P. Tapponnier, N. Arnaud, L. Bourjot, J. P. Avouac, P. Vidal, L. Qing, P. Yusheng, and W. Yi, Tectonics of western Tibet, between the Tarim and the Indus, *Earth Planet. Sci. Lett.*, *142*, 311–330, 1996.

Mattern, F., W. Schneider, Y. Li, and X. Li, A traverse through the western Kunlun (Xinjiang, China): Tentative geodynamic implications for the Paleozoic and Mesozoic, *Geol. Fundsch.*, *85*, 705–722, 1996.

McDonough, W. F., Constraints on the composition of the

continental lithospheric mantle, *Earth Planet. Sci. Lett.*, *101*, 1–18, 1990.

McDonough, W. F., and S.-S. Sun, Composition of the Earth, *Chem. Geol.*, *120*, 223–253, 1995.

McKenna, L. W., and J. D. Walker, Geochemistry of crustally derived leucocratic igneous rocks from the Ulugh Muztagh area, northern Tibet and their implications for the formation of the Tibetan Plateau, *J. Geophys. Res.*, *95*, 21,483–21,502, 1990.

McKenzie, D., ^{230}Th-^{238}U disequilibria and the melting processes beneath ridge axes, *Earth Planet. Sci. Lett.*, *72*, 149–157, 1985.

Miller, C., R. Schuster, U. Klötzli, W. Frank, and F. Purtscheller, Post-collisional potassic and ultrapotassic magmatism in SW Tibet: Geochemical and Sr-Nd-Pb-O isotopic constraints for mantle source characteristics and petrogenesis, *J. Petrol.*, *40*(9), 1399–1424, 1999.

Molnar, P., P. England, and J. Martinod, Mantle dynamics, uplift of the Tibetan Plateau, and the Indian Monsoon, *Rev. Geophys.*, *31*(4), 357–396, 1993.

Mukasa, S. B., and H. G. Wilshire, Isotopic and trace element compositions of upper mantle and lower crustal xenoliths, Cima volcanic field, California: Implications for evolution of the subcontinental lithospheric mantle, *J. Geophys. Res.*, *102*, 20,133–20,148, 1997.

Nelson, K. D., et al., Partially molten middle crust beneath southern Tibet: Synthesis of project INDEPTH results, *Science*, *274*, 1684–1688, 1996.

Owens, T. J., and G. Zandt, Implications of crustal property variations for models of Tibetan plateau evolution, *Nature*, *387*, 37–43, 1997.

Patiño Douce, A. E., and J. S. Beard, Dehydration-melting of biotite gneiss and quartz amphibolite from 3 to 15 kbar, *J. Petrol.*, *36*(3), 707–738, 1995.

Patiño Douce, A. E., and T. C. McCarthy, Melting of crustal rocks during continental collision and subduction, in *When Continents Collide: Geodynamics and Geochemistry of Ultrahigh-Pressure Rocks*, edited by B. R. Hacker and J. G. Liou, pp. 27–55, Kluwer Acad., Norwell, Mass., 1998.

Pearce, J. A., and H. Mei, Volcanic rocks of the 1985 geotraverse: Lhasa to Golmud, *Philos. Trans. R. Soc. London*, *327*, 169–201, 1988.

Pertermann, M., and M. M. Hirschmann, Consequences of fertile pyroxenites in basalt source regions, *Eos Trans. AGU, Suppl.*, *81*(48), F1284, 2000.

Pickett, D. A., and M. T. Murrell, Observations of ^{231}Pa/^{235}U disequilibrium in volcanic rocks, *Earth Planet. Sci. Lett.*, *148*, 259–271, 1997.

Pietruszka, A. J., K. H. Rubin, and M. O. Garcia, ^{226}Ra-^{230}Th-^{238}U disequilibria of historical Kilauea lavas (1790–1982) and the dynamics of mantle melting within the Hawaiian plume, *Earth Planet. Sci. Lett.*, *186*, 15–31, 2001.

Qi, Q., L. A. Taylor, and X. Zhou, Petrology and geochemistry of mantle peridotite xenoliths from SE China, *J. Petrol.*, *36*(1), 55–79, 1995.

Qin, Z. W., Disequilibrium partial melting model and implications for the fractionations of trace elements during mantle melting, *Earth Planet. Sci. Lett.*, *112*, 75–90, 1992.

Rapp, R. P., and E. B. Watson, Dehydration melting of metabasalt at 8–32 kbar: Implications for continental growth and crust–mantle recycling, *J. Petrol.*, *36*(4), 891–931, 1995.

Reid, M. R., Processes of mantle enrichment and magmatic differentiation in the eastern Snake River Plain: Th isotope evidence, *Earth Planet. Sci. Lett.*, *131*, 239–254, 1995.

Reid, M. R., and F. C. Ramos, Chemical dynamics of enriched mantle in the southwestern United States: Thorium isotope evidence, *Earth Planet. Sci. Lett.*, *138*, 67–81, 1996.

Reiners, P. W., Temporal-compositional trends in intraplate basalt eruptions: Implications for mantle heterogeneity and melting processes, *Geochem. Geophys. Geosyst.*, *3*(2), 1011, 10.1029/2001GC000250, 2002.

Rushmer, T., An experimental deformation study of partially molten amphibolite: Application to low-melt fraction segregation, *J. Geophys. Res.*, *100*, 15,681–15,695, 1995.

Ryerson, F. J., G. Peltzer, P. Tapponnier, R. C. Finkel, A.-S. Meriaux, J. Van der Woerd, and M. W. Caffee, Active slip-rates on the Altyn Tagh Fault Karakax Valley Segment: Constraints from surface exposure dating, *Eos Trans. AGU*, *80*(46), F1008, 1999.

Salters, V., and J. Longhi, Trace element partitioning during the initial stages of melting beneath mid-ocean ridges, *Earth Planet. Sci. Lett.*, *166*, 15–30, 1999.

Sen, C., and T. Dunn, Dehydration melting of a basaltic composition amphibolite at 1.5 and 2.0 GPa: Implications for the origins of adakites, *Contrib. Mineral. Petrol.*, *117*, 394–409, 1994.

Sengor, A. M. C., East Asian tectonic collage, *Nature*, *318*, 16–17, 1985.

Silver, P., Seismic anisotropy beneath the continents: Probing the depths of geology, *Annu. Rev. Earth Planet. Sci.*, *24*, 385–4432, 1996.

Sims, K. W., D. J. DePaolo, M. T. Murrell, W. S. Baldridge, S. J. Goldstein, and D. A. Clague, Mechanisms of magma generation beneath Hawaii and mid-ocean ridges: Uranium/thorium and samarium/neodymium isotopic evidence, *Science*, *267*, 508–512, 1995.

Sims, K. W. W., D. J. DePaolo, M. T. Murrell, W. S. Baldridge, S. Goldstein, D. Clague, and M. Jull, Porosity of the melting zone and variations in solid mantle upwelling rate beneath Hawaii: Inferences from ^{238}U-^{230}Th-^{226}Ra and ^{235}U-^{231}Pa disequilibria, *Geochim. Cosmochim. Acta*, *63*, 4119–4138, 1999.

Spiegelman, M., and T. Elliott, Consequences of melt transport for uranium series disequilibria, *Earth Planet. Sci. Lett.*, *118*, 1–20, 1993.

Stracke, A., V. J. M. Salters, and K. W. W. Sims, Assessing the presence of garnet–pyroxenite in the mantle sources of basalts through combined hafnium–neodymium–thorium isotope systematics, *Geochem. Geophys. Geosyst.*, 10.1029/1999GC000013, 1999.

Sturm, M. E., S. J. Goldstein, E. M. Klein, J. A. Karson, and M. T. Murrell, Uranium-series age constraints on lavas from the axial valley of the Mid-Atlantic Ridge, MARK area, *Earth Planet. Sci. Lett.*, *181*, 61–70, 2000.

Tapponnier, P., Z. Xu, F. Roger, B. Meyer, N. Arnaud, G.

Wittlinger, and J. Yang, Oblique stepwise rise and growth of the Tibet Plateau, *Science*, *294*, 1671–1677, 2001.

Tatsumoto, M., A. R. Basu, W. Huang, J. Wang, and G. Xie, Sr, Nd, and Pb isotopes of ultramafic xenoliths in volcanic rocks of Eastern China: Enriched components EMI and EMII in subcontinental lithosphere, *Earth Planet. Sci. Lett.*, *113*, 107–128, 1992.

Thomas, L. E., C. J. Hawkesworth, P. Van Calsteren, S. P. Turner, and N. W. Rogers, Melt generation beneath ocean islands: A U-Th-Ra isotope study from Lanzarote in the Canary Islands, *Geochim. Cosmochim. Acta*, *63*, 4081–4099, 1999.

Turner, S., C. Hawkesworth, J. Liu, N. Rogers, S. Kelley, and P. van Calsteren, Timing of Tibetan uplift constrained by analysis of volcanic rocks, *Nature*, *364*, 50–54, 1993.

Turner, S., N. Arnaud, J. Liu, N. Rogers, C. Hawkesworth, N. Harris, S. Kelley, P. van Calsteren, and W. Deng, Post-collision, shoshonitic volcanism on the Tibetan plateau: Implications for convective thinning of the lithosphere and the source of ocean island basalts, *J. Petrol.*, *37*(1), 45–71, 1996.

Turner, S., J. Blundy, B. Wood, and M. Hole, Large ^{230}Th-excesses in basalts produced by partial melting of spinel lherzolite, *Chem. Geol.*, *162*, 127–136, 2000a.

Turner, S. P., R. M. M. George, P. J. Evans, C. J. Hawkesworth, and G. F. Zellmer, Time-scales of magma formation, ascent and storage beneath subduction-zone volcanoes, *Philos. Trans. R. Soc. London, Ser. A*, *358*, 1443–1464, 2000b.

Van Orman, J. A., T. L. Grove, and N. Shimizu, Uranium and thorium diffusion in diopside, *Earth Planet. Sci. Lett.*, *160*, 505–519, 1998.

van Westrenen, W., J. Blundy, and B. Wood, Crystal-chemical controls on trace element partitioning between garnet and anhydrous silicate melt, *Am. Mineral.*, *84*(5–6), 838–847, 1999.

van Westrenen, W., J. D. Blundy, and B. J. Wood, High field strength element/rare earth element fractionation during partial melting in the presence of garnet: Implications for identification of mantle heterogeneities, *Geochem. Geophys. Geosyst.*, *2*, 10.1029/2000GC000133, 2001.

Volpe, A. M., and S. J. Goldstein, ^{226}Ra-^{230}Th disequilibrium in axial and off-axis mid-ocean ridge basalts, *Geochim. Cosmochim. Acta*, *57*, 1233–1242, 1993.

Watson, E. B., and T. M. Harrison, Zircon saturation revisited: Temperature and composition effects in a variety of crustal magma types, *Earth Planet. Sci. Lett.*, *64*, 295–304, 1983.

Wei, W., et al., Detection of widespread fluids in the Tibetan crust by magnetotelluric studies, *Science*, *292*, 716–718, 2001.

Williams, R. W., and J. B. Gill, Effects of partial melting on the uranium decay series, *Geochim. Cosmochim. Acta*, *53*, 1607–1619, 1989.

Williams, R. W., K. D. Collerson, J. B. Gill, and C. Deniel, High Th/U ratios in subcontinental lithospheric mantle: Mass spectrometric measurements of Th isotopes in Gaussberg lamproites, *Earth Planet. Sci. Lett.*, *111*, 257–268, 1992.

Williams, R. W., and J. B. Gill, Th isotope and U-series disequilibria in some alkali basalts, *Geophys. Res. Lett.*, *19*(2), 139–142, 1992.

Wittlinger, G., P. Tapponnier, G. Poupinet, J. Mei, S. Danian, G. Herquel, and F. Masson, Tomographic evidence for localized lithospheric shear along the Altyn Tagh fault, *Science*, *282*, 74–76, 1998.

Wood, B. J., J. D. Blundy, and J. A. C. Robinson, The role of clinopyroxene in generating U-series disequilibrium during mantle melting, *Geochim. Cosmochim. Acta*, *63*, 1613–1620, 1999.

Yin, A., and T. M. Harrison, Geologic evolution of the Himalayan–Tibetan orogen, *Annu. Rev. Earth Planet. Sci.*, *28*, 211–280, 2000.

Yin, A., and S. Nie, A Phanerozoic palinspastic reconstruction of China and its neighboring regions, in *The Tectonic Evolution of Asia*, edited by A. Yin and T. M. Harrison, pp. 442–485, Cambridge Univ. Press, New York, 1996.

Yin, A., T .M. Harrison, and F. J. Ryerson, Transtension along the left-slip Altyn Tagh and Kunlun faults as a mechanism for the occurrence of Late Cenozoic volcanism in the northern Tibetan Plateau, *Eos Trans. AGU*, 567, 1995.

Zellmer, G., S. Turner, and C. Hawkesworth, Timescales of destructive plate margin magmatism: New insights from Santorini, Aegean volcanic arc, *Earth Planet. Sci. Lett.*, *174*, 265–281, 2000.

Zindler, A., and S. Hart, Chemical geodynamics, *Annu. Rev. Earth Planet. Sci.*, *14*, 493–571, 1986.

Zou, H., Trace element fractionation during modal and nonmodal dynamic melting and open-system melting: A mathematical treatment, *Geochim. Cosmochim. Acta*, *62*, 137–195, 1998.

Zou, H., and A. Zindler, Theoretical studies of ^{238}U-^{230}Th-^{226}Ra and ^{235}U-^{231}Pa disequilibria in young lavas produced by mantle melting, *Geochim. Cosmochim. Acta*, *64*, 1809–1817, 2000.